NASA TN D-1060

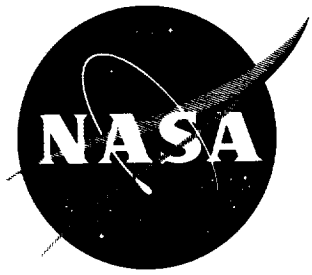

TECHNICAL NOTE

D-1060

AERODYNAMIC-DERIVATIVE CHARACTERISTICS OF THE X-15 RESEARCH AIRPLANE AS DETERMINED FROM FLIGHT TESTS FOR MACH NUMBERS FROM 0.6 TO 3.4

By Roxanah B. Yancey, Herman A. Rediess, and Glenn H. Robinson

Flight Research Center
Edwards, Calif.

NATIONAL AERONAUTICS AND SPACE ADMINISTRATION

WASHINGTON January 1962

NATIONAL AERONAUTICS AND SPACE ADMINISTRATION

TECHNICAL NOTE D-1060

AERODYNAMIC-DERIVATIVE CHARACTERISTICS OF THE X-15 RESEARCH AIRPLANE AS DETERMINED FROM FLIGHT TESTS FOR MACH NUMBERS FROM 0.6 TO 3.4

By Roxanah B. Yancey, Herman A. Rediess, and Glenn H. Robinson

SUMMARY

The longitudinal, lateral, and directional stability and control derivatives as determined from flight tests of the X-15 research airplane with an interim rocket engine are presented for Mach numbers from 0.6 to 3.4 and angles of attack up to 16°. The results are derived from pulse, pull-up, and sideslip maneuvers and are compared with wind-tunnel results for corresponding Mach number and angle-of-attack conditions. The various methods used in the analysis of the flight data are considered, and new methods are described in detail.

Comparisons of the flight and wind-tunnel results show that, for the most part, the predicted levels of stability and control effectiveness were realized under full-scale flight conditions. For Mach numbers in excess of 1.8, however, the static directional-stability derivative and the directional control effectiveness from wind-tunnel data are as much as 25 percent higher than values determined from flight. The dihedral effect, as predicted, diminishes with increasing supersonic Mach number and becomes adverse at Mach numbers above 2.3. Significant variations due to angle of attack or jet-exhaust effects could not be detected in the flight data, except for the dihedral derivative which shows a possible angle-of-attack effect.

Where the suitability of the flight records for simple analysis was questionable, an analog-matching technique was also applied. The effects of the stability augmentation system on the flight responses were approximated, where necessary, by relatively simple empirical factors derived from an X-15 flight simulator.

INTRODUCTION

Flight simulators are necessarily being used more extensively than in the past for planning and directing flight test programs with

experimental and research-type airplanes. An accurate simulation of the airplane response characteristics, however, necessitates a complete compilation of the characteristics of the stability and control derivatives which are indicative of the actual airplane. In this respect, flight-determined derivatives obtained during the buildup of the flight tests are compared to wind-tunnel data to ascertain the degree of correlation and to safeguard against unforeseen characteristics.

It is of general interest, then, to compare the wind-tunnel data employed in the simulation program for the X-15 airplane with data derived from actual flight tests in a hypersonic flight research program being conducted by the National Aeronautics and Space Administration, the U. S. Air Force, and the U. S. Navy at the NASA Flight Research Center, Edwards, Calif. H 2 2 8

This paper summarizes the stability and control derivatives that were obtained during the interim buildup flight program with the X-15 in which the low-power LR11 Reaction Motors rocket engines were used. The methods and flight techniques employed to obtain derivatives are discussed briefly, and the flight data are compared with predictions from wind-tunnel tests. The results from this interim program serve as a basis for extending the flight envelope of the X-15 to the hypersonic flight regimes.

A detailed derivation of the particular relationships used for determining the directional-stability, dihedral, and yaw-damping derivatives is presented in appendix A, by Chester H. Wolowicz of the Flight Research Center.

SYMBOLS AND COEFFICIENTS

The results of this investigation are referred to the body system of orthogonal axes.

a_n normal acceleration at center of gravity, g units

a_t transverse acceleration at center of gravity, g units

b wing span, ft

C_l rolling-moment coefficient, $\frac{\text{Rolling moment}}{\bar{q}Sb}$

C_{l_p} damping-in-roll derivative, $\frac{\partial C_l}{\partial\left(\frac{pb}{2V}\right)}$, per radian

C_{l_r} rate of change of rolling-moment coefficient with yawing angular-velocity factor, $\frac{\partial C_l}{\partial\left(\frac{rb}{2V}\right)}$, per radian

C_{l_β} lateral-stability derivative, $\frac{\partial C_l}{\partial \beta}$, per deg

$C_{l_{\delta_a}}$ aileron-effectiveness derivative, $\frac{\partial C_l}{\partial \delta_a}$, per deg

$C_{l_{\delta_v}}$ variation of rolling-moment coefficient with vertical-tail deflection, $\frac{\partial C_l}{\partial \delta_v}$, per deg

C_m pitching-moment coefficient, $\frac{\text{Pitching moment}}{\bar{q}S\bar{c}}$

$\left(C_{m_q} + C_{m_{\dot{\alpha}}}\right)$ damping-in-pitch derivative, $\frac{\partial C_m}{\partial\left(\frac{q\bar{c}}{2V}\right)} + \frac{\partial C_m}{\partial\left(\frac{\dot{\alpha}\bar{c}}{2V}\right)}$, per radian

C_{m_α} longitudinal-stability derivative, $\frac{\partial C_m}{\partial \alpha}$, per deg

$C_{m_{\delta_h}}$ stabilizer-effectiveness derivative, $\frac{\partial C_m}{\partial \delta_h}$, per deg

C_N normal-force coefficient, $\frac{\text{Normal force}}{\bar{q}S}$

C_{N_α} normal-force-curve slope, $\frac{\partial C_N}{\partial \alpha}$, per deg

$C_{N_{\alpha_T}}$ normal-force-curve slope for pull-up, $\left(\frac{dC_N}{d\alpha}\right)_T = \frac{\partial C_N}{\partial \alpha} + \frac{\partial C_N}{\partial \delta_h}\frac{d\delta_h}{d\alpha}$, per deg

C_n yawing-moment coefficient, $\frac{\text{Yawing moment}}{\bar{q}Sb}$

C_{n_p} variation of yawing-moment coefficient with rolling angular-velocity factor, $\frac{\partial C_n}{\partial\left(\frac{pb}{2V}\right)}$, per radian

$\left(C_{n_r} - C_{n_{\dot{\beta}}}\right)$ damping-in-yaw derivative, $\frac{\partial C_n}{\partial\left(\frac{rb}{2V}\right)} - \frac{\partial C_n}{\partial\left(\frac{\dot{\beta}b}{2V}\right)}$, per radian

C_{n_β} directional-stability derivative, $\frac{\partial C_n}{\partial \beta}$, per deg

$C_{n_{\delta_a}}$ variation of yawing-moment coefficient with aileron deflection, $\frac{\partial C_n}{\partial \delta_a}$, per deg

$C_{n_{\delta_v}}$ vertical-tail-effectiveness derivative, $\frac{\partial C_n}{\partial \delta_v}$, per deg

C_Y side-force coefficient, $\frac{\text{Side force}}{\bar{q}S}$

C_{Y_β} side-force derivative, $\frac{\partial C_Y}{\partial \beta}$, per deg

$C_{Y_{\delta_v}}$ variation of side-force coefficient with vertical-tail deflection, $\frac{\partial C_Y}{\partial \delta_v}$, per deg

$\bar{c}$ mean aerodynamic chord, ft

F_h longitudinal center-stick force, lb

F_1, F_3 correction factors to the natural frequency for stability-augmentation-system effects (eqs. (B9) and (B11))

F_2, F_4 correction factors to the damping for stability-augmentation-system effects (eqs. (B9) and (B11))

F_5 correction factor to $\frac{|r|}{|\beta|}$ for stability-augmentation-system effects (eq. (B11))

g	acceleration due to gravity, ft/sec^2
h_p	pressure altitude, ft
I_X	moment of inertia about X-axis, $slug\text{-}ft^2$
I_Y	moment of inertia about Y-axis, $slug\text{-}ft^2$
I_Z	moment of inertia about Z-axis, $slug\text{-}ft^2$
I_{XZ}	product of inertia, $\frac{1}{2}\left(I_Z - I_X\right)\sin 2\epsilon$, $slug\text{-}ft^2$
K	stability-augmentation-system gain
M	Mach number
M	dimensional pitching-moment parameter (appendix B), $\frac{\bar{q}S\bar{c}}{I_Y} C_m$, $1/sec^2$
m	mass of airplane, slugs
P	period of longitudinal or lateral-directional oscillation, sec
p	rolling angular velocity, radians/sec or deg/sec
q	pitching angular velocity, radians/sec or deg/sec
$\bar{q}$	free-stream dynamic pressure, $\frac{1}{2}\rho V^2$, lb/sq ft
R	Reynolds number
r	yawing angular velocity, radians/sec or deg/sec
S	wing area, sq ft
s	Laplace transform variable, 1/sec
$T_{1/2}$	time required for transient oscillation to damp to half amplitude, sec
t	time, sec
V	true airspeed, ft/sec
W	airplane weight, lb
Z	dimensional lift parameter, $-\frac{\bar{q}S}{mV} C_N$, 1/sec

α airplane angle of attack, deg

β airplane angle of sideslip, deg

Δ incremental value

δ_a total aileron deflection, $\delta_{h_L} - \delta_{h_R}$, deg

δ_{a_β} rate of change of aileron deflection with sideslip angle

δ_h horizontal-tail deflection, $\frac{1}{2}\left(\delta_{h_L} + \delta_{h_R}\right)$, deg

δ_v vertical-tail deflection, $\frac{1}{2}\left(\delta_{v_u} + \delta_{v_l}\right)$, deg

δ_{v_β} rate of change of vertical-tail deflection with sideslip angle

ϵ inclination of principal X-axis to the body X-axis, deg

ζ ratio of actual damping to critical damping

θ pitch attitude, deg

τ time constant for simplified stability augmentation system, sec

ρ mass density of air, slugs/cu ft

Φ phase angle, deg

Φ_d damping angle, $\tan^{-1}\frac{\zeta}{\sqrt{1 - \zeta^2}}$, deg

φ roll attitude, deg

ω_n undamped natural frequency of airplane in longitudinal or lateral-directional mode, radians/sec

ω_{n_d} damped natural frequency, $\omega_n\sqrt{1 - \zeta^2}$, radians/sec

Subscripts:

L left

l lower vertical tail

q partial derivative with respect to pitching rate (appendix B)

R	right
T	pull-up maneuver with respect to lift-curve slope
u	upper vertical tail
α	partial derivative with respect to angle of attack
δ_h	partial derivative with respect to stabilizer deflection
θ	longitudinal mode
ψ	lateral-directional mode
0	initial term

A dot over a symbol indicates the derivative of the quantity with respect to time.

The symbol $| \; |$ represents the absolute magnitude of a quantity. The phase angle of a vector x relative to a reference vector y is indicated by the subscript xy.

A prime indicates that the term was obtained with the stability augmentation system in operation (see appendix B).

A bar over a term (with the exception of $\bar{q}$) denotes that the term was obtained on the X-15 simulator (see appendix B).

AIRPLANE

The X-15 airplane (figs. 1 and 2) is a single-place research rocket airplane designed to investigate the hypersonic flight regime at speeds up to 6,600 feet per second and at altitudes up to at least 250,000 feet. The major part of the X-15 cylindrical fuselage is composed of integral propellant tanks, thereby requiring the addition of triangular-shaped side fairings to enclose the components of the various systems. An instrument compartment is located immediately to the rear of the cockpit. Speed brakes are provided in the rear inboard sections of the upper and lower vertical tails. The landing gear consists of a dual-wheel nose gear located well forward and a skid-type main gear located under the tail.

For the tests reported herein, except as specified in particular instances, the X-15 was equipped with two LR11 rocket engines

manufactured by the Reaction Motors Division of the Thiokol Chemical Corp. The engines are mounted one above the other in the rear end of the X-15 fuselage. Each engine has four individually operated cylinders which use an alcohol-water mixture as fuel and liquid oxygen as an oxidizer. The combined thrust of the engines is about 16,000 pounds at an altitude of 50,000 feet. The design altitude of the nozzles is 19,000 feet.

The X-15 has a 5-percent wing with an aspect ratio of 2.5, a wedge-type vertical tail, and a slab-type horizontal surface. The physical characteristics of the airplane are listed in detail in table I. The variations with airplane weight of the moments of inertia about the body reference axes for both power-off and power-on conditions, as determined by the manufacturer, are shown in figure 3.

Irreversible hydraulic systems actuate all aerodynamic control surfaces of the X-15. Landing flaps are provided which also are hydraulically actuated. A slab-type horizontal stabilizer furnishes longitudinal control when deflected symmetrically and lateral control when deflected differentially. The horizontal-control-surface rate is limited to 25 degrees per second, and the time lag from stick to surface movement is about 0.04 second. The upper and lower directional-control surfaces are moved by conventional rudder pedals. The lower movable section is jettisoned prior to landing to provide adequate ground clearance.

A rate-sensing damper system coupled to the aerodynamic-control surfaces provides three-axes stability augmentation. An interconnect damper system (termed "yar") feeds yaw-rate signals into the roll-control surfaces to provide extra roll damping. The gains and authority of the pitch, roll, yaw, and yar damper systems are shown in table II. For convenience, the stability augmentation system is referred to herein as "SAS".

INSTRUMENTATION

The following quantities pertinent to the derivative investigation were recorded on standard NASA internal recording instruments synchronized at 0.1-second intervals by a common timer:

Airspeed and pressure altitude
Normal and transverse accelerations
Pitching angular velocity and acceleration
Yawing angular velocity and acceleration
Rolling angular velocity and acceleration
Angle of attack

Angle of sideslip
Right and left horizontal-tail deflection
Upper and lower vertical-tail deflection

The airspeed and altitude were measured by a NASA pitot-static tube mounted on the airplane nose boom. Angles of attack and sideslip were measured by free-floating vanes also mounted on the nose boom. The errors in these angles, induced by the aircraft pitching, yawing, or rolling motions, were found to be within the experimental accuracy of the data; hence, corrections were not considered necessary. Reference was made to the airplane body axes in determining the angular velocities and accelerations as well as the linear acceleration.

The ranges and dynamic characteristics for the instruments measuring linear acceleration, angle of attack, angle of sideslip, angular velocity, and acceleration are as follows:

Function	Range	Undamped natural frequency, cps	Damping ratio
a_n, g units	-3.0 8.0	31.0	0.640
a_t, g units	±1.0	9.5	.640
α, deg	-20.0 40.0	12.0	.700
β, deg	±30.0	12.0	.700
q, radians/sec	±0.5	8.5	.630
p, radians/sec	±2.0	15.0	.602
r, radians/sec	±0.5	8.5	.666
$\dot{q}$, radians/sec^2	±1.0	19.5	.685
$\dot{r}$, radians/sec^2	±1.6	20.0	.646
$\dot{p}$, radians/sec^2	±3.2	19.8	.640

Recordings were generally accurate within ±2 percent of the full-scale readings.

An inertial platform was available on many flights for supplementary measurement of altitude and velocity as well as airplane attitudes about all three earth-referenced axes.

FLIGHT TESTS

The X-15 airplane is carried under the right wing of a B-52 airplane to an altitude of approximately 45,000 feet and released to perform its flight mission. It then glides to a landing on the dry lakebed at Edwards Air Force Base, Calif.

The flight data used in determining the derivative characteristics presented herein consisted of time histories of the airplane responses to abrupt pitch-, yaw-, and roll-control inputs (pulses), and to pull-up and sideslip maneuvers performed at Mach numbers from 0.6 to 3.4. For the pulses, the pilot applied control rapidly, returned the control to the trim position, then attempted to hold the controls fixed during the ensuing transient motions. A typical time history of a pitch pulse is shown in figure 4. In lateral-directional maneuvers the roll control was difficult to hold fixed; therefore, most of the yaw and roll pulses had some roll-control input during the transient oscillations. Time histories of yaw and roll pulses with the stability augmentation system off and on are shown in figures 5(a) to 5(d). Ideally, pulse maneuvers should be performed at constant Mach number and altitude, and the free oscillations should be allowed to persist through a large number of cycles following the control input; however, typical X-15 missions and performance characteristics generally precluded attainment of these ideal conditions. Thus, it was usually necessary to restrict the number and duration of the maneuvers that could be performed in any one flight. Moreover, the stability augmentation system often could not be completely deactivated because of safety-of-flight restrictions, and the controls-fixed condition could not be realized. The lowest gain settings possible were used for these conditions, and an empirical correction to the basic data was applied to account for the effects of the stability augmentation system (see appendix B).

Pull-ups and wind-up turns, as dictated by flight patterns, were also used to extract static longitudinal-derivative characteristics. A time history of a typical pull-up maneuver is shown in figure 6.

A limited number of wings-level sideslip maneuvers were performed as an alternate technique for determining the static lateral-directional characteristics. A time history of a typical sideslip is shown in figure 7.

The maneuvers were performed for the overall ranges of flight conditions of $M = 0.6$ to 3.4, $h_p = 23{,}000$ ft to 80,000 ft, $\bar{q} = 130$ lb/sq ft to 1,300 lb/sq ft, $\alpha = 0°$ to 16°, and $a_n = 0g$ to $3.5g$.

WIND-TUNNEL DATA

Derivative characteristics from X-15 model tests in the Mach number range from 0.2 to 3.4 are available from several sources (refs. 1 to 8). The manufacturer, in reference 1, has assimilated the various wind-tunnel test results into a composite set of faired aerodynamic data extending through most of the predicted flight envelope. The wind-tunnel data presented herein as a comparison with flight data are

faired values based on reference 1 and the references listed in the following tabulation. All the data are for trim horizontal-stabilizer settings, and C_{m_α}, $C_{m_{\delta_h}}$, $C_{n_{\delta_v}}$, and C_{n_β} have been corrected to a center-of-gravity position at 22 percent of the mean aerodynamic chord.

Reference	Facility	Mach number range	Model scale	$R \times 10^{-6}$
2	Langley full-scale and free-flight tunnels	Low speed	1/7, 1/10	0.43 to 0.55
3	Ames 12-foot pressure wind tunnel	0.22 to 0.92	0.09	.75 to 1.5
4	Langley 4- by 4-foot supersonic pressure tunnel	1.41, 2.01	.02	.46 to .71
5	Ames Unitary Plan wind tunnel	1.55 to 3.50	.09	1.5
6	Langley Unitary Plan wind tunnel	2.29, 2.98, 4.65	.067	.51 to 4.43
7	Naval Supersonic Laboratory Wind Tunnel	1.5, 2.5, 3.5	.02	.34 to .39
8	Naval Supersonic Laboratory Wind Tunnel	1.5, 2.5, 3.5	.02	.34 to .39

Unpublished data from the Langley 8-foot transonic pressure tunnel for the 0.067-scale model were also used in determining the fairings over a Mach number range from 0.60 to 1.18 ($2.2 \times 10^6 < R < 2.8 \times 10^6$).

ANALYSIS AND PRESENTATION OF FLIGHT DATA

The relationships generally employed for determining the longitudinal derivatives from flight data may be found in various studies, for example, reference 9. It was recognized during the development of the X-15 airplane, however, that difficulties would probably be experienced in obtaining flight data which would be of acceptable quality for use in the more comprehensive methods of determining the lateral derivatives. As a result, a study was made of the limitations of normally used simplified equations, applicable to oscillatory data, for determining

C_{n_β} and $\left(C_{n_r} - C_{n_{\dot\beta}}\right)$. During the study, new expressions were developed for C_{n_β}, C_{l_β}, and $\left(C_{n_r} - C_{n_{\dot\beta}}\right)$ which are applicable when the influence of I_{XZ} is negligible, as is the case for the X-15. The development and limitations of these expressions and the limitations of the previously used expressions are presented in appendix A.

The extent of the flight coverage in this paper relative to the predicted overall flight envelope is shown in figure 8. Data at high angles of attack are generally lacking; however, data obtained from flights with the XLR99 engine will gradually fill out the flight envelope.

The following sections briefly outline the analytical methods and equations used for calculating the longitudinal and lateral-directional derivatives and describe an analog-matching technique for verification of the calculated results. A figure showing the variation of the flight-determined derivative with Mach number is introduced after each equation is presented.

Longitudinal Derivatives

The derivatives C_{N_α}, C_{m_α}, and $\left(C_{m_q} + C_{m_{\dot\alpha}}\right)$ for fixed controls were determined from the following relationships (refs. 9 and 10)

$$C_{N_\alpha} = \frac{W}{\bar{q}S}\frac{|a_n|}{|\alpha|} \tag{1}$$

$$C_{m_\alpha} = -\frac{I_Y}{\bar{q}S\bar{c}}\omega_n^2 \tag{2}$$

$$\omega_n^2 = \omega_{n_d}^2 + \left(\zeta\omega_n\right)^2$$

$$= \left(\frac{2\pi}{P}\right)^2 + \left(\frac{0.693}{T_{1/2}}\right)^2$$

$$\left(C_{m_q} + C_{m_{\dot\alpha}}\right) = \frac{4VI_Y}{\bar{q}S\bar{c}}\left(\frac{C_{N_\alpha}\bar{q}S}{2mV} - \zeta\omega_n\right) \tag{3}$$

The derivative $C_{N_{\alpha_T}}$ corresponding to near-trimmed flight conditions was determined as the linear variation of normal-force lift coefficient with angle of attack during pull-ups or turns.

The basic values of P, $T_{1/2}$, and amplitude ratio $\frac{|a_n|}{|\alpha|}$ used in these expressions are presented in table III. The values were derived from time histories similar to those shown in figure 4. When the stability augmentation system was in operation, the undamped natural frequency ω_n and damping parameter $\zeta\omega_n$ obtained from the time histories were corrected to approximately the SAS-off values by the method presented in appendix B. The computed values for C_{N_α}, C_{m_α}, $\left(C_{m_q} + C_{m_{\dot{\alpha}}}\right)$, and $C_{m_{\delta_h}}$ are plotted as functions of Mach number in figure 9. In figures 10(a), 10(b), 11, and 12, respectively, C_{N_α}, $C_{N_{\alpha_T}}$, C_{m_α}, and $\left(C_{m_q} + C_{m_{\dot{\alpha}}}\right)$ are compared with wind-tunnel predictions.

H 228

The control effectiveness $C_{m_{\delta_h}}$ was determined from quantities measured during the initial input portion of the stabilizer pulse maneuvers. The following simplified expression was used

$$C_{m_{\delta_h}} = \frac{1}{\Delta\delta_h}\left(\frac{I_Y}{\bar{q}S\bar{c}}\Delta\dot{q} - C_{m_\alpha}\Delta\alpha\right) \tag{4}$$

When C_{m_α} could not be obtained from flight data at identical conditions of M and α, an estimated value from faired data was used. The flight and wind-tunnel results are compared in figure 13.

Lateral and Directional Derivatives

The graphical time-vector method (ref. 9) has generally been used at the NASA Flight Research Center for determining lateral-stability derivatives. In applying this method, however, good-quality control-fixed transient responses at near-constant Mach number and angle of attack are normally required. Since such conditions were rarely achieved with the X-15, simpler analytical expressions were used in this paper, with few exceptions, in place of the time-vector method.

The static directional-stability derivative C_{n_β} was determined from the following equation (see appendix A)

$$C_{n_\beta} = \frac{I_Z\omega_n}{\bar{q}Sb}\frac{|r|}{|\beta|} \tag{5}$$

Occasionally, accurate estimates of the ratio $\left|\frac{r}{\beta}\right|$ could not be determined from the flight records, and the expression

$$C_{n_\beta} = \frac{I_Z \omega_n^2}{\bar{q}Sb} + \alpha \frac{I_Z}{I_X} C_{l_\beta} \tag{6}$$

was used instead. In this expression, a value for C_{l_β} was obtained from faired flight data, if available, or wind-tunnel data. Where sideslips were performed and the lateral- and directional-control effectiveness were known from flight tests, the following relationship was applied

H 2 2 8

$$C_{n_\beta} = -\left(C_{n_{\delta_v}} \delta_{v_\beta} + C_{n_{\delta_a}} \delta_{a_\beta}\right) \tag{7}$$

The dihedral effect C_{l_β} was evaluated from both pulse and sideslip maneuvers. For pulses (appendix A)

$$C_{l_\beta} = \frac{1}{\alpha}\left[\frac{I_X}{\bar{q}Sb} \omega_n^2 \left(\left|\frac{r}{\beta}\right| \frac{1}{\omega_n} - 1\right)\right] \tag{8}$$

For sideslips

$$C_{l_\beta} = -\left(C_{l_{\delta_v}} \delta_{v_\beta} + C_{l_{\delta_a}} \delta_{a_\beta}\right) \tag{9}$$

where the control-effectiveness terms were taken from fairings of previous flight data.

Table IV summarizes the basic values of P, $T_{1/2}$, and $\left|\frac{r}{\beta}\right|$ from which the derivatives C_{n_β} and C_{l_β} were computed. Figure 5 presents typical time histories of the vertical-tail and aileron pulses that were analyzed. The flight-determined derivatives are plotted as functions of Mach number in figure 14. Flight-determined values of C_{n_β} and C_{l_β} are compared with wind-tunnel results in figures 15 and 16, respectively.

The control-effectiveness derivatives were determined from measured increments of the yaw and roll accelerations and velocities during the initial control inputs. The directional-control derivatives $C_{n_{\delta_v}}$ and $C_{l_{\delta_v}}$ were calculated from the following expressions

$$C_{n_{\delta_v}} = \frac{1}{\Delta\delta_v}\left(\frac{I_Z}{\bar{q}Sb}\Delta\dot{r} - \frac{I_{XZ}}{\bar{q}Sb}\Delta\dot{p} - C_{n_\beta}\Delta\beta\right) \tag{10}$$

$$C_{l_{\delta_v}} = \frac{1}{\Delta\delta_v}\left(\frac{I_X}{\bar{q}Sb}\Delta\dot{p} - \frac{I_{XZ}}{\bar{q}Sb}\Delta\dot{r} - C_{l_p}\frac{\Delta pb}{2V} - C_{l_\beta}\Delta\beta\right) \tag{11}$$

and the roll-control derivatives from similar expressions

$$C_{n_{\delta_a}} = \frac{1}{\Delta\delta_a}\left(\frac{I_Z}{\bar{q}Sb}\Delta\dot{r} - \frac{I_{XZ}}{\bar{q}Sb}\Delta\dot{p} - C_{n_\beta}\Delta\beta\right) \tag{12}$$

$$C_{l_{\delta_a}} = \frac{1}{\Delta\delta_a}\left(\frac{I_X}{\bar{q}Sb}\Delta\dot{p} - \frac{I_{XZ}}{\bar{q}Sb}\Delta\dot{r} - C_{l_p}\frac{\Delta pb}{2V} - C_{l_\beta}\Delta\beta\right) \tag{13}$$

In the absence of flight-determined values for C_{l_p}, wind-tunnel values were used. Results for these derivatives are shown as functions of Mach number in figure 17. The control-effectiveness derivatives determined in flight are compared with wind-tunnel predictions in figures 18 and 19.

The side-force derivative C_{Y_β} was computed for pulses from the simple expression

$$C_{Y_\beta} = -\frac{W}{\bar{q}S}\frac{|a_t|}{|\beta|} \tag{14}$$

and for sideslips with wings near level

$$C_{Y_\beta} = \frac{W}{\bar{q}S}\frac{da_t}{d\beta} - C_{Y_{\delta_v}}\frac{d\delta_v}{d\beta} \tag{15}$$

This derivative is shown as a function of Mach number in figure 14. The flight and wind-tunnel data for C_{Y_β} are given in figure 20.

Lastly, the approximate equation (appendix A)

$$\left(C_{n_r} - C_{n_{\dot{\beta}}}\right) = -\frac{I_Z}{\left(\frac{b}{2V}\right)\bar{q}Sb}\zeta\omega_n \tag{16}$$

was used for the damping derivative. These derivatives are presented in figures 14 and 21.

The derivatives C_{n_p} and C_{l_r} for the X-15 are very small and, because of limitations in the techniques employed, could not be determined. During the interim program, the roll maneuvers were not of sufficient duration and rate to enable a satisfactory evaluation of the damping derivative C_{l_p}.

When the stability augmentation system is operative, as it was during many of the test maneuvers, the preceding relationships for the transient maneuvers are not directly applicable. The manner in which the basic flight data ω_n, $\zeta\omega_n$, and $\frac{|r|}{|\beta|}$ were corrected for the stability-augmentation-system effects to make them usable in the foregoing equations is described in appendix B.

H 2 2 8

Analog-Matching Technique

The preceding equations (eqs. (1) to (16)) are not generally applicable where pilot-induced or pilot-plus-SAS-induced control motions followed the initial control input, inasmuch as they are derived from control-fixed airplane oscillations following the forcing control input. Therefore, derivatives were extracted from these types of flight data by a matching technique (ref. 11). This technique was also employed occasionally to confirm results from the simplified equations.

A simulation of the flight time history for each maneuver was obtained on a five-degree-of-freedom analog setup by programing the control inputs into the analog through a plotting table and comparing the resultant simulated airplane responses to a transparent overlay of the actual flight records. The stability and control derivatives on the simulator were then varied from the basic wind-tunnel values, as necessary, to match the flight time history. Figures 22 and 23 are typical analog matches of an aileron-induced lateral-directional oscillation and a horizontal-stabilizer pulse, respectively. The values of derivatives which gave the best match for each maneuver are presented with analytical results in figures 10(a), 11 to 13, 15, 16, 18, 19, and 21.

A further refinement, particularly important because of the rapidly changing flight conditions experienced during such maneuvers, was the simulation of flight dynamic pressure as a linear function of time.

When the stability-augmentation-system gains were moderate to high, the basic airplane damping derivatives contributed only a small percentage of the total damping, and, therefore, could not be determined with sufficient accuracy to be considered conclusive. In each case, only derivatives which made a significant change in the time history were considered. These, in general, included all the derivatives in the

longitudinal mode and the lateral-directional mode except C_{n_p}, C_{l_r}, C_{l_β}, and C_{Y_β}. The derivatives $\left(C_{m_q} + C_{m_{\dot{\alpha}}}\right)$ and $\left(C_{n_r} - C_{n_{\dot{\beta}}}\right)$ could usually be determined from maneuvers performed with the corresponding stability augmentation system disengaged.

RESULTS AND DISCUSSION

In the following sections, the general trends in the derivative characteristics from flight are considered briefly and comparisons are made with wind-tunnel predictions. The accuracy of the flight-determined derivatives for any one method of analysis can best be ascertained by the scatter of data in the figures. It is difficult and possibly unrealistic to express the accuracies as a definite percentage value because of the multitude of factors involved, such as the quality of the maneuver, the accuracy of the sensing and recording instruments, the accuracy of the equation or the technique for the particular condition being investigated, and the skill of the analyst who weighs all of the factors in the analysis.

Basic Data

The periods, times to damp to half amplitude, and amplitude ratios obtained from time histories of pulses over the range of flight conditions covered by the X-15 with the LR11 engines are listed in tables III and IV. Because the flight parameters which influence the basic data (Mach number, angle of attack, altitude, power on or off, SAS on or off, and combination of SAS gain settings) varied continuously within each flight and from flight to flight, different flight conditions were experienced for almost every data point. It is estimated that the periods could generally be determined within 0.05 second for the low to moderate damping ratios encountered (less than 0.30).

Longitudinal Derivatives

Flight trends.- The longitudinal stability and control derivatives from flight, as shown in figure 9, exhibit the moderate compressibility and transonic Mach number effects expected for slender vehicles and the gradual decline of lift effectiveness with increasing supersonic Mach number. The stability derivative C_{m_α} reaches a peak value at a somewhat higher Mach number and, in particular, changes less rapidly with Mach number than does $C_{m_{\delta_h}}$ at transonic speeds. These combined effects produce an apparent pitch-up while the airplane is decelerating

through this range. The values of C_{m_α} and $C_{m_{\delta_h}}$ indicate that the X-15 has a high level of static longitudinal stability and control effectiveness throughout the Mach number and angle-of-attack ranges covered. The dynamic stability is moderately high in the transonic region, but, as indicated by the trends of $\left(C_{m_q} + C_{m_{\dot{\alpha}}}\right)$ and C_{N_α}, decreases to low levels with increasing supersonic Mach number. Although several ranges of angle of attack are shown in the figure, no consistent angle-of-attack effect is apparent within the experimental accuracy of the data. A distinction between power-on and power-off conditions is also made in figure 9; however, no consistent trend due to power is evident.

Wind-tunnel predictions.- The flight results are compared with wind-tunnel predictions for several angle-of-attack ranges in figures 10 to 13. The method for determining the derivatives and the use of stability augmentation (on or off) are also indicated in these figures. In general, the flight and wind-tunnel results are in fairly close agreement. A comparison of figures 10(a) and 10(b) for the pulse- and pull-up type maneuvers, respectively, reveals an appreciable reduction in airplane lift-curve slope due to the relatively large negative stabilizer lift required for trim. The stabilizer effectiveness from flight (fig. 13), however, appears to be about 10 percent lower than the wind-tunnel values in the lower range of stabilizer deflections. The static stability derivative C_{m_α} is higher than predicted at angles of attack from 0° to 4° (fig. 11). At Mach numbers from 1.2 to 2.0, flight-determined C_{m_α} does not verify the nonlinear effect of angle of attack that is evident in the wind-tunnel results at low angles of attack. The flight data are relatively constant with angle of attack, whereas the wind-tunnel values of C_{m_α} decrease slightly at low angles of attack in this Mach number range.

Figure 10(a) and figures 11 to 13 show that the results from the analog-matching technique generally agree with the results from the simplified equations discussed previously.

Lateral-Directional Derivatives

Flight trends.- The directional-stability derivative C_{n_β} from flight tests, as seen in figure 14, reaches a maximum value at $M \approx 1.4$ and diminishes rapidly in the Mach number range from 1.6 to 2.0. Although the values of C_{n_β} at angles of attack from 10° to 16° appear lower than at other angles of attack (fig. 14), there are not sufficient data to draw a definite conclusion relative to angle-of-attack effect. Data obtained from subsequent flights, but not included in this paper,

show that the downward trend in C_{n_β}, as established by this interim program, does not continue but tends to level off at higher Mach numbers. No systematic effect of engine power is apparent in the C_{n_β} flight data. All data beyond $M \approx 2.0$ were obtained after engine shutdown. At high Mach numbers it appears that angle of attack may affect the dihedral derivative C_{l_β} (fig. 14); however, the trends cannot be firmly established because of a lack of data in this area. The flight-determined C_{l_β} gradually changes from favorable to adverse (positive C_{l_β}) at about $M = 2.3$ and possibly tends to increase positively with angle of attack at Mach numbers greater than 2.3. In flight, this trend is evident at the higher angles of attack as a reduction of the airplane static stability in the Dutch roll mode (ref. 12) and as a change in the relation of bank angle to sideslip, which results in poor lateral controllability when the pilot attempts to control the airplane in the normal manner (ref. 13). There was no apparent power effect on C_{l_β}. The derivative C_{Y_β} conforms generally with the trends for C_{n_β}. Figure 14 also shows a gradual deterioration of the damping-in-yaw derivative $\left(C_{n_r} - C_{n_{\dot\beta}}\right)$ as Mach number increases.

The control derivatives $C_{n_{\delta_v}}$, $C_{l_{\delta_v}}$, $C_{n_{\delta_a}}$, and $C_{l_{\delta_a}}$ in figure 17 are also characterized by peak magnitudes in the transonic range and declining trends with increasing Mach number with little, if any, effect of angle of attack or engine power. Subsequent data not included in the $C_{n_{\delta_v}}$ plots show, as for C_{n_β}, that the downward trend in the curve tends to level off in the higher Mach number range rather than to continue in the direction indicated by the data from the interim-engine flights. The derivative $C_{l_{\delta_v}}$, similar to C_{l_β}, reverses sign at $M \approx 2.3$. This effect is attributed to an increasing effectiveness of the lower-vertical-tail surface at positive angles of attack and high Mach numbers (ref. 14) and is the primary factor necessitating the addition of the "yar" crossover signal in the stability augmentation system (see AIRPLANE section).

Wind-tunnel predictions.- Figures 15, 16, and 18 to 21 present comparisons of the flight-determined derivatives with wind-tunnel data. Where the wind-tunnel data indicated a possible sensitivity to angle of attack, various ranges of angle of attack are presented. The method of analysis and the type of maneuver analyzed (control pulse or sideslip) are indicated in the figures. Figures 15 and 16 for C_{n_β} and C_{l_β}, respectively, generally reveal a sparsity of data at the higher angles of attack where flight responses suitable for derivative analysis were usually more difficult to obtain. At low angles of attack and at Mach numbers between 1.2 and 1.8, the flight-determined directional-stability derivatives are higher than the wind-tunnel prediction by approximately

H 2 2 8

10 percent; however, above $M = 1.8$ the directional stability appears to be lower than predicted by as much as 20 to 25 percent. The cause for these discrepancies has not been firmly established, but is believed to be the result of a reduction in vertical-tail effectiveness due, possibly, to aeroelastic effects. Little, if any, distinction is apparent between the results for the dynamic (pulse-type) and steady-state (sideslip) maneuvers. The flight results for C_{l_β} show a greater degree of scatter than for C_{n_β}, but are generally in accord with the wind-tunnel values for angles of attack between 0° and 8°. Sparsity of the data at high angles of attack precludes correlating flight and wind-tunnel data in this area. The damping derivatives in figure 21 also agree with the wind-tunnel results, although some points obtained with the stability augmentation system engaged show appreciable scatter. It should be noted, however, that the stability-augmentation-system correction (as discussed in appendix B) for this derivative is often as large or larger than the derivative itself and is, thus, cause for considerable uncertainty.

The control derivatives from flight and wind-tunnel tests are compared in figures 18 and 19. Angle-of-attack effects for these derivatives are not significant; hence, the wind-tunnel curves for only the mean angle of attack are shown. The flight values of $C_{n_{\delta_v}}$ (fig. 18) show a low trend at Mach numbers greater than 1.6, similar to that for C_{n_β} (fig. 15). The agreement in the results for the lateral-control derivatives in figure 19 is fairly good, although considerable scatter in the results for $C_{n_{\delta_a}}$ is evident above a Mach number of 2.0.

CONCLUSIONS

A flight investigation of the X-15 stability and control derivatives in the Mach number range from 0.6 to 3.4 has revealed the following:

1. The levels of longitudinal and directional static stability and control effectiveness are relatively high for angles of attack up to 16°; whereas, the longitudinal and directional dynamic stability with the stability augmentation system inoperative are generally low. The principal derivatives show a gradual decline with increasing supersonic Mach number.

2. Angle of attack has little discernible effect on the principal derivatives, with the possible exception of the lateral-stability derivative C_{l_β}.

3. The effective dihedral gradually diminishes with increasing Mach number, becoming adverse at Mach numbers greater than 2.3.

4. Engine power has no discernible effect on the principal derivatives.

5. The wind-tunnel predictions generally agree well with flight data, except that the directional stability and control derivatives from wind-tunnel tests are 20 to 25 percent high in the low angle-of-attack range at Mach numbers greater than 1.8.

6. The simplified equations derived for the analysis of the X-15 flight data and the analog techniques employed for reducing the data obtained with the stability augmentation system in operation are effective in coping with the available data and provide reasonably accurate and consistent results.

H
2
2
8

7. The stability augmentation system produces small, but correctable, increases in the frequency of the transient responses and substantial increases in damping. The damping derivatives, therefore, are less reliably obtained with the stability augmentation system engaged.

Flight Research Center
National Aeronautics and Space Administration
Edwards, Calif., September 20, 1961

APPENDIX A

APPROXIMATE EQUATIONS FOR DETERMINING C_{n_β}, C_{l_β}, and $\left(C_{n_r} - C_{n_{\dot{\beta}}}\right)$

By Chester H. Wolowicz

The familiar expressions used to calculate the derivatives C_{n_β} and $\left(C_{n_r} - C_{n_{\dot{\beta}}}\right)$ from flight data are considered in order to illustrate their drawbacks and limitations. Subsequently, forms better suited to the X-15 analysis are derived which, in turn, define a more convenient relationship for determination of the dihedral effect C_{l_β}.

Limitations of Commonly Used Expressions for C_{n_β} and $\left(C_{n_r} - C_{n_{\dot{\beta}}}\right)$

To evaluate the limitations of normally accepted expressions for C_{n_β}, the following expression was derived based on the solution of the determinant of the linearized lateral and directional equations of motion. (The expression includes all but the most negligible quantities.)

$$\left(1 - \frac{I_{XZ}}{I_X}\sin\alpha\right)C_{n_\beta} \approx \frac{I_Z}{\bar{q}Sb}\left[\omega_n^2 - \left(2\zeta\omega_n\right)^2 + 2\zeta\omega_n\left(\frac{g\sin\theta}{V} - C_{Y_\beta}\frac{\bar{q}S}{mV}\right)\right]$$

$$- \left(\frac{I_{XZ}}{I_Z} - \sin\alpha\right)\frac{I_Z}{I_X}C_{l_\beta} - \frac{b}{2V}\left\{2\zeta\omega_n\left[\frac{I_Z}{I_X}\left(C_{l_p} + C_{l_{\dot{\beta}}}\sin\alpha\right)\right.\right.$$

$$\left.\left. + \left(C_{n_r} - C_{n_{\dot{\beta}}}\right)\right] + C_{l_p}\left(C_{n_r} - C_{n_{\dot{\beta}}}\right)\frac{\bar{q}Sb}{I_X}\frac{b}{2V}\right\} + \frac{b}{2V}\left[\left(\frac{g\sin\theta}{V}\right.\right.$$

$$\left.\left. - C_{Y_\beta}\frac{\bar{q}S}{mV}\right)\left(C_{n_r} + C_{l_p}\frac{I_Z}{I_X}\right) + \frac{g\cos\theta}{V}C_{l_\beta}C_{n_r}\frac{\bar{q}Sb}{I_X\omega_n^2}\right] \tag{A1}$$

A study of this equation shows that when C_{n_β} is small, that is, of the order of 0.0014 per degree or less, the ordinarily insignificant damping terms become important. In such instances C_{l_p} and $\left(C_{n_r} - C_{n_{\dot{\beta}}}\right)$ are significant.

When C_{n_β} is of a higher order than 0.0014, as for the X-15, the damping terms in equation (A1) may be ignored and a workable approximate equation used. Also, if the angle-of-attack range is restricted so that $\sin \alpha \approx \alpha$, and if the term $\frac{I_{XZ}}{I_X} \sin \alpha$ becomes a negligibly small second-order quantity, then

$$C_{n_\beta} \approx \frac{I_Z \omega_n^2}{\bar{q}Sb} + \alpha \frac{I_Z}{I_X} C_{l_\beta} \tag{A2}$$

That C_{n_β} is a function of C_{l_β} in equation (A2) does not make this equation too desirable if C_{l_β} is estimated from wind-tunnel data rather than from flight data. This is especially true when the vertical tail is subject to such factors as jet-exhaust effects and flexibility; for such conditions, the value of C_{l_β} may be appreciably different from wind-tunnel data.

The following equation has been used often (ref. 9) to obtain $\left(C_{n_r} - C_{n_{\dot\beta}}\right)$

$$\left(C_{n_r} - C_{n_{\dot\beta}}\right) \approx - \frac{2I_Z}{b^2}\left(\frac{2\zeta\omega_n V}{\bar{q}S} + \frac{C_{Y_\beta}}{m}\right) \tag{A3}$$

The use of equation (A3) is restricted to angles of attack less than about 4°, primarily because of the omission of C_{l_p}.

Development of New Expressions for C_{n_β} and $\left(C_{n_r} - C_{n_{\dot\beta}}\right)$ Applicable to the X-15 Airplane

Where the influences of I_{XZ} and C_{n_p} are negligible, as on the X-15 airplane, the yawing-moment equation for control-fixed conditions reduces to

$$\frac{I_Z}{\bar{q}Sb} \dot{r} - \left(C_{n_r} - C_{n_{\dot\beta}}\right)\frac{rb}{2V} - C_{n_\beta}\beta = 0 \tag{A4}$$

For a transient oscillatory sinusoidal motion, $\dot{r}$, r, and β can be replaced by the following expressions

$$\left.\begin{aligned}
\dot{r} &= \frac{|\dot{r}|}{|r|} r_0 e^{-\zeta\omega_n t}\cos\left(\omega_{n_d} t + \Phi_{\dot{r}r}\right) = \omega_n r_0 e^{-\zeta\omega_n t}\cos\left(\omega_{n_d} t + \frac{\pi}{2} + \Phi_d\right) \\
r &= \frac{|r|}{|r|} r_0 e^{-\zeta\omega_n t}\cos\left(\omega_{n_d} t + \Phi_{rr}\right) = r_0 e^{-\zeta\omega_n t}\cos\,\omega_{n_d} t \\
\beta &= \frac{|\beta|}{|r|} r_0 e^{-\zeta\omega_n t}\cos\left(\omega_{n_d} t + \Phi_{\beta r}\right)
\end{aligned}\right\} \quad (A5)$$

H
2
2
8

Substituting equation (A5) for $\dot{r}$, r, and β in equation (A4), expanding by trigonometric identities, and regrouping

$$\left(-\frac{I_Z}{\bar{q}Sb}\omega_n \cos\Phi_d + C_{n_\beta}\frac{|\beta|}{|r|}\sin\Phi_{\beta r}\right)\sin\omega_{n_d} t$$

$$-\left[\frac{I_Z}{\bar{q}Sb}\omega_n \sin\Phi_d + \left(C_{n_r} - C_{n_{\dot{\beta}}}\right)\frac{b}{2V} + C_{n_\beta}\frac{|\beta|}{|r|}\cos\Phi_{\beta r}\right]\cos\omega_{n_d} t = 0 \quad (A6)$$

The first parenthesized term is a summation of components perpendicular to the r vector; the second parenthesized term is a summation of components parallel to the r vector. Hence

$$-\frac{I_Z}{\bar{q}Sb}\omega_n \cos\Phi_d + C_{n_\beta}\frac{|\beta|}{|r|}\sin\Phi_{\beta r} = 0 \quad (A7)$$

and

$$\frac{I_Z}{\bar{q}Sb}\omega_n \sin\Phi_d + \left(C_{n_r} - C_{n_{\dot{\beta}}}\right)\frac{b}{2V} + C_{n_\beta}\frac{|\beta|}{|r|}\cos\Phi_{\beta r} = 0 \quad (A8)$$

The phase angle $\Phi_{\beta r}$, on the basis of vector diagrams using X-15 wind-tunnel data, appears to vary from 90° at $\alpha = 0°$ to about 92° at $\alpha = 18°$. Also, the damping angle is small. Thus

$$\left.\begin{aligned}
&\sin\Phi_{\beta r} \approx 1 \qquad \cos\Phi_d \approx 1 \\
\text{and} \quad &\omega_n \sin\Phi_d = \zeta\omega_n
\end{aligned}\right\} \quad (A9)$$

Hence, substituting equation (A9) into equations (A7) and (A8)

$$C_{n_\beta} \approx \frac{I_Z}{\bar{q}Sb} \frac{|r|}{|\beta|} \omega_n \tag{A10}$$

and

$$\left(C_{n_r} - C_{n_{\dot{\beta}}}\right) \approx -\frac{2V}{b} \zeta\omega_n \frac{I_Z}{\bar{q}Sb} + C_{n_\beta} \frac{|\beta|}{|r|} \cos \Phi_{\beta r} \tag{A11}$$

Because $\Phi_{\beta r}$ will vary only a small amount from 90°, as mentioned previously, more error will be introduced in equation (A11) by attempting to use values of $\Phi_{\beta r}$ as determined from flight data than will be present by omitting the expression $C_{n_\beta} \frac{|\beta|}{|r|} \cos \Phi_{\beta r}$. The quality of the flight data precludes the successful determination of $\Phi_{\beta r}$ to better than about 4° or 5°. Hence, the more practical consideration of equation (A11) would be to reduce it to

$$\left(C_{n_r} - C_{n_{\dot{\beta}}}\right) \approx -\zeta\omega_n \frac{I_Z}{\left(\frac{b}{2V}\right)\bar{q}Sb} \tag{A12}$$

The elimination of the C_{n_β} term in equation (A11) to form equation (A12) results in slightly larger negative values of $\left(C_{n_r} - C_{n_{\dot{\beta}}}\right)$ than if the term had been retained and accurate values of $\Phi_{\beta r}$ could be determined. Whereas equation (A3) cannot be used at angles of attack above about 4°, equation (A12) is workable up to angles of attack of approximately 12°.

Development of an Approximate Expression for C_{l_β}

Simplified expressions for determining C_{l_β} that can be generally used have not been developed successfully. However, for the X-15 where the influence of I_{XZ} is negligible, it is possible to combine equations (A2) and (A10) to obtain

$$C_{l_\beta} \approx \frac{1}{\alpha} \frac{I_X \omega_n^2}{\bar{q}Sb} \left(\frac{|r|}{|\beta|} \frac{1}{\omega_n} - 1 \right) \tag{A13}$$

This equation is limited in its application in that it should not be used when C_{n_β} is small, as noted in the discussion of equation (A2);

also, it generally may not be satisfactory when the angle of attack is less than about 4°. At angles of attack less than about 4°, $\frac{|r|}{|\beta|}\frac{1}{\omega_n}$ may approach 1.0, and the error in reading $\frac{|r|}{|\beta|}$ from the flight records may result in an error in $\frac{|r|}{|\beta|}\frac{1}{\omega_n}$ which may exceed the net magnitude of the parenthesized quantity. Also, at very low angles of attack, the error in the flight-determined values of α can produce large errors in the equation. As α approaches zero, equation (A13) approaches an indeterminant form.

APPENDIX B

CORRECTIONS FOR THE EFFECTS OF THE STABILITY AUGMENTATION SYSTEM IN THE DETERMINATION OF STABILITY DERIVATIVES FROM FLIGHT DATA

The principal flight-motion parameters needed to calculate the static and dynamic stability derivatives from flight data are the undamped natural frequency ω_n and the damping parameter $\zeta\omega_n$. When a pulse is performed with the stability augmentation system engaged, the resulting period, as well as the time to damp to one-half amplitude, is in general different than with the stability augmentation system inoperative, as shown in figures 24 and 25. The primary difference in the periods is attributed to time lags and nonlinearities in the augmentation system and not to an increased damping ratio ζ; in fact, the change in period due to the system response is in the opposite direction from that caused by an increase in damping ratio. For example, in figures 24 and 25 the SAS-on period is shorter than the SAS-off period, even though the damping ratio with the SAS on is larger than the SAS-off damping ratio. The relationship of period to the undamped natural frequency and the damping ratio is

$$P = \frac{2\pi}{\omega_n\sqrt{1 - \zeta^2}} \tag{B1}$$

From this equation it is evident that for a constant undamped natural frequency ω_n, an increase in ζ will give a longer period, rather than a shorter period as shown in figures 24 and 25. To satisfy equation (B1), therefore, the undamped natural frequency must have changed when the stability augmentation system was engaged.

The differences in ω_n and $\zeta\omega_n$ for the stability augmentation system engaged and disengaged are demonstrated qualitatively in the following section by expanding the characteristic equation for the longitudinal short-period mode with the stability-augmentation-system transfer function approximated by means of a simple first-order time lag. The longitudinal mode is used for this illustration since it reduces to a simpler expression than the lateral-directional mode; however, the effect is similar. Following this illustration, the actual method used to correct for the stability-augmentation-system effects is discussed.

The Longitudinal Short-Period Mode

The Laplace transformed two-degree-of-freedom longitudinal equations of motion for a rigid aircraft perturbating about a mean flight path are

$$\left[s - M_q\right] q(s) + \left[-M_\alpha\right] \alpha(s) = M_{\delta_h} \delta_h(s) \tag{B2}$$

$$\left[-1\right] q(s) + \left[s - Z_\alpha\right] \alpha(s) = Z_{\delta_h} \delta_h(s) \tag{B3}$$

With no pilot control input, the transfer function for a damper with a first-order time lag may be expressed as

$$\frac{\delta_h(s)}{q(s)} = \frac{K}{1 + \tau s} \tag{B4}$$

$$\approx K(1 - \tau s) \tag{B5}$$

Substituting equation (B5) into equations (B2) and (B3) leads to the following determinant

$$\begin{vmatrix} \left[\left(1 + M_{\delta_h} K\tau\right) s + \left(-M_q - M_{\delta_h} K\right)\right] & \left(-M_\alpha\right) \\ \left[\left(Z_{\delta_h} K\tau\right) s + \left(-1 - Z_{\delta_h} K\right)\right] & \left(s - Z_\alpha\right) \end{vmatrix} = 0 \tag{B6}$$

The solution to equation (B6) gives the characteristic equation of the short-period longitudinal mode

$$s^2 + \frac{1}{1 + M_{\delta_h} K\tau} \left(-Z_\alpha - M_q - M_{\delta_h} K - Z_\alpha M_{\delta_h} K\tau + M_\alpha Z_{\delta_h} K\tau\right) s$$

$$+ \frac{1}{1 + M_{\delta_h} K\tau} \left(-M_\alpha + Z_\alpha M_q + Z_\alpha M_{\delta_h} K - M_\alpha Z_{\delta_h} K\right) = 0 \tag{B7}$$

Only the first three terms of the first parenthesized quantity and the first term in the second parenthesized quantity of equation (B7)

are significant for the X-15. The frequency and damping are then given by

$$\left(\omega_{n\theta}'\right)^2 \approx \frac{-M_\alpha}{1 + M_{\delta_h} K\tau} = \frac{|M_\alpha|}{1 - \left|M_{\delta_h} K\tau\right|} \tag{B8}$$

$$2\zeta_\theta'\omega_{n\theta}' \approx \frac{-Z_\alpha - M_q - M_{\delta_h} K}{1 + M_{\delta_h} K\tau} = \frac{\left|Z_\alpha + M_q + M_{\delta_h} K\right|}{1 - \left|M_{\delta_h} K\tau\right|} \tag{B9}$$

With the pitch damper off ($K = 0$), $\omega_{n\theta}' = \omega_{n\theta}$ and $\zeta_\theta' = \zeta_\theta$. With the pitch damper on ($K > 0$), it can be seen from equations (B8) and (B9) that $\omega_{n\theta}'$ and particularly $\zeta_\theta'\omega_{n\theta}'$ (due to the $M_{\delta_h} K$ term in the numerator will be greater than $\omega_{n\theta}$ and $\zeta_\theta\omega_{n\theta}$, respectively. Therefore, the values of these terms from flight must be corrected before they can be used in equations (2) and (3) to determine C_{m_α} and $\left(C_{m_q} + C_{m_{\dot\alpha}}\right)$.

If the damper were a first-order linear system, a fairly simple analytical correction to $\omega_{n\theta}'$ and $\zeta_\theta'\omega_{n\theta}'$ could be made. However, the system in the X-15 is approximately fifth order and also very nonlinear; thus, any analytical correction which might be derived for this system would be complex. Therefore, the following semiempirical method was devised for correcting $\omega_{n\theta}'$ and $\zeta_\theta'\omega_{n\theta}'$.

The X-15 fixed-base simulator, which employs a duplicate of the X-15 control system and stability augmentation system (ref. 15), was found to be the most convenient and accurate means for obtaining corrections to $\omega_{n\theta}'$ and $\zeta_\theta'\omega_{n\theta}'$. Correction factors F_1 and F_2 were determined for each flight value of $\omega_{n\theta}'$ and $\zeta_\theta'\omega_{n\theta}'$, respectively, by reproducing as closely as possible the actual flight conditions on the simulator, and by performing two longitudinal pulses of approximately the same magnitude, one with the stability augmentation system operating at the same gain as in flight and the other with the stability augmentation system off. From the analog time histories of the pulses (fig. 24) the SAS-off natural frequency $\bar\omega_{n\theta}$ and damping $\bar\zeta_\theta\bar\omega_{n\theta}$ and the SAS-on frequency $\bar\omega_{n\theta}'$ and damping $\bar\zeta_\theta'\bar\omega_{n\theta}'$ were obtained and applied as corrections to the flight SAS-on data as follows

$$F_1 = \left(\frac{\bar\omega_{n\theta}}{\bar\omega_{n\theta}'}\right)^2 \qquad F_2 = \frac{\bar\zeta_\theta\bar\omega_{n\theta}}{\bar\zeta_\theta'\bar\omega_{n\theta}'} \tag{B10}$$

$$\omega_n^2 \approx F_1\left(\omega_{n\theta}'\right)^2 \qquad \zeta\omega_n \approx F_2\left(\zeta_\theta'\omega_{n\theta}'\right) \tag{B11}$$

Figure 26 shows the effect of this correction as applied to the derivatives C_{m_α} and $\left(C_{m_q} + C_{m_{\dot{\alpha}}}\right)$.

Dutch Roll Mode

Flight-data corrections for stability-augmentation-system effects similar to those discussed in the preceding section are also required for the Dutch roll mode. An analytical explanation of the nature of this correction, therefore, is not repeated.

In general, the same empirical method was used for the Dutch roll mode, with one addition. The primary equations used in this paper to calculate C_{n_β} and C_{l_β} (eqs. (5) and (8)) both use the parameter $\frac{|r|}{|\beta|}$ which must also be corrected for stability-augmentation-system effects. Corrections to $\frac{|r'|}{|\beta'|}$ as well as to ω_{n_ψ}' and $\zeta_\psi'\omega_{n_\psi}'$ were obtained from analog time histories (fig. 25) and applied as follows

$$F_3 = \left(\frac{\bar{\omega}_{n_\psi}}{\bar{\omega}_{n_\psi}'}\right)^2 \qquad F_4 = \frac{\bar{\zeta}_\psi \bar{\omega}_{n_\psi}}{\bar{\zeta}_\psi' \bar{\omega}_{n_\psi}'} \qquad F_5 = \frac{|\bar{r}|}{|\bar{\beta}|} \frac{|\bar{\beta}'|}{|\bar{r}'|} \tag{B12}$$

$$\omega_n^2 = F_3\left(\omega_{n_\psi}'\right)^2 \qquad \zeta\omega_n \approx F_4\left(\zeta_\psi'\omega_{n_\psi}'\right) \qquad \frac{|r|}{|\beta|} \approx F_5 \frac{|r'|}{|\beta'|} \tag{B13}$$

Figure 27 shows the effect of this correction on the terms C_{n_β}, C_{l_β}, $\left(C_{n_r} - C_{n_{\dot{\beta}}}\right)$.

REFERENCES

1. Anon.: Revised Basic Aerodynamic Characteristics of the X-15 Research Airplane. Rep. NA-59-1203, (Contract AF 33(600)-31693), North American Aviation, Inc., Aug. 7, 1959.

2. Hassell, James L., Jr., and Hewes, Donald E.: Investigation of the Subsonic Stability and Control Characteristics of a 1/7-Scale Model of the North American X-15 Airplane With and Without Fuselage Forebody Strakes. NASA TM X-210, 1960.

3. Lopez, Armando E., and Tinling, Bruce E.: The Static and Dynamic-Rotary Stability Derivatives at Subsonic Speeds of a Model of the X-15 Research Airplane. NACA RM A58F09, 1958.

4. Driver, Cornelius: Effect of Forebody Strakes on the Aerodynamic Characteristics in Pitch and Sideslip of a Hypersonic Airplane Configuration at Mach Numbers of 1.41, 2.01, and 6.86. NASA TM X-116, 1959.

5. Tunnell, Phillips J., and Latham, Eldon A.: The Static and Dynamic-Rotary Stability Derivatives of a Model of the X-15 Research Airplane at Mach Numbers From 1.55 to 3.50. NASA Memo 12-23-58A, 1959.

6. Franklin, Arthur E., and Lust, Robert M.: Investigation of the Aerodynamic Characteristics of a 0.067-Scale Model of the X-15 Airplane (Configuration 3) at Mach Numbers of 2.29, 2.98, and 4.65. NASA TM X-38, 1959.

7. Anon.: A Third Series of Supersonic Force Tests on the Full-Span Model X-15 for North American Aviation, Inc. WTR 228, M.I.T. Naval Supersonic Lab., Nov. 1958.

8. Anon.: A Fourth Series of Supersonic Force Tests on the Full-Span Model X-15 for North American Aviation, Incorporated. WTR 239, M.I.T. Naval Supersonic Lab., Dec. 1958.

9. Wolowicz, Chester H., and Holleman, Euclid C.: Stability-Derivative Determination From Flight Data. AGARD Rep. No. 224, 1958.

10. Andrews, William H., and Rediess, Herman A.: Flight-Determined Stability and Control Derivatives of a Supersonic Airplane With a Low-Aspect-Ratio Unswept Wing and a Tee-Tail. NASA Memo 2-2-59H, 1959.

11. Triplett, William C., Brown, Stuart C., and Smith, G. Allan: The Dynamic-Response Characteristics of a 35° Swept-Wing Airplane as Determined From Flight Measurements. NACA Rep. 1250, 1955.

12. Moul, Martin T., and Paulson, John W.: Dynamic Lateral Behavior of High-Performance Aircraft. NACA RM L58E16, 1958.

13. Taylor, Lawrence W., Jr.: Analysis of a Pilot-Airplane Lateral Instability Experienced With the X-15 Airplane. NASA TN D-1059, 1961.

14. Walker, Harold J., and Wolowicz, Chester H.: Theoretical Stability Derivatives for the X-15 Research Airplane at Supersonic and Hypersonic Speeds Including a Comparison With Wind-Tunnel Results. NASA TM X-287, 1960.

15. Hughes, R. O., Weis, J. P., and Hoffman, D. P.: Flight Simulation of the X-15 Research Airplane in Unlimited Six Degrees of Freedom. Rep. NA 60-437, North American Aviation, Inc., July 5, 1960.

TABLE I.- PHYSICAL CHARACTERISTICS OF THE X-15 AIRPLANE

Wing:	
Airfoil section	NACA 66005 (Modified)
Total area (includes 94.98 sq ft covered by fuselage), sq ft	200
Span, ft	22.36
Mean aerodynamic chord, ft	10.27
Root chord, ft	14.91
Tip chord, ft	2.98
Taper ratio	0.20
Aspect ratio	2.50
Sweep at 25-percent chord line, deg	25.64
Incidence, deg	0
Dihedral, deg	0
Aerodynamic twist, deg	0
Flap -	
Type	Plain
Area (each), sq ft	8.30
Span (each), ft	4.50
Inboard chord, ft	2.61
Outboard chord, ft	1.08
Deflection, maximum down, deg	40
Ratio flap chord to wing chord	0.22
Ratio total flap area to wing area	0.08
Ratio flap span to wing semispan	0.40
Trailing-edge angle, deg	5.67
Sweepback angle of hinge line, deg	0
Horizontal tail:	
Airfoil section	NACA 66005 (Modified)
Total area (includes 63.29 sq ft covered by fuselage), sq ft	115.34
Span, ft	18.08
Mean aerodynamic chord, ft	7.05
Root chord, ft	10.22
Tip chord, ft	2.11
Taper ratio	0.21
Aspect ratio	2.83
Sweep at 25-percent chord line, deg	45
Dihedral, deg	-15
Ratio horizontal-tail area to wing area	0.58
Movable-surface area, sq ft	51.77
Deflection -	
Longitudinal, up, deg	15
Longitudinal, down, deg	35
Lateral differential (pilot authority), deg	±15
Lateral differential (autopilot authority), deg	±30
Control system	Irreversible hydraulic boost with artificial feel

TABLE I.- PHYSICAL CHARACTERISTICS OF THE X-15 AIRPLANE (Concluded)

Upper vertical tail:	
Airfoil section	10° single wedge
Total area, sq ft	40.91
Span, ft	4.58
Mean aerodynamic chord, ft	8.95
Root chord, ft	10.21
Tip chord, ft	7.56
Taper ratio	0.74
Aspect ratio	0.51
Sweep at 25-percent chord line, deg	23.41
Ratio vertical-tail area to wing area	0.20
Movable-surface area, sq ft	26.45
Deflection, deg	±7.50
Sweepback of hinge line, deg	0
Control system	Irreversible hydraulic boost with artificial feel
Lower vertical tail:	
Airfoil section	10° single wedge
Total area, sq ft	34.41
Span, ft	3.83
Mean aerodynamic chord, ft	9.17
Root chord, ft	10.21
Tip chord, ft	8
Taper ratio	0.78
Aspect ratio	0.43
Sweep at 25-percent chord line, deg	23.41
Ratio vertical-tail area to wing area	0.17
Movable-surface area, sq ft	19.95
Deflection, deg	±7.50
Sweepback of hinge line, deg	0
Control system	Irreversible hydraulic boost with artificial feel
Fuselage:	
Length, ft	50.75
Maximum width, ft	7.33
Maximum depth, ft	4.67
Maximum depth over canopy, ft	4.97
Side area (total), sq ft	215.66
Fineness ratio	10.91
Speed brake (typical for each of four):	
Area (each), sq ft	5.57
Span (each), ft	1.67
Chord (each), ft	3.33
Deflection, deg	35
Center-of-gravity location, percent mean aerodynamic chord	22 ±1
	Launch / Landing
Weight, lb	33,500 / 14,600

H-228

TABLE II.- GAIN AND AUTHORITY OF THE X-15 STABILITY AUGMENTATION SYSTEM

Switch position	Gain							
	Pitch		Roll		Yaw		Yar	
	In./deg/sec	Deg/deg/sec	In./deg/sec	Deg/deg/sec	In./deg/sec	Deg/deg/sec	In./deg/sec	Deg/deg/sec
1	0.005	0.075	0.0017	0.051	0.004	0.03	0.003	0.09
2	.010	.150	.0033	.100	.008	.06	.006	.18
3	.015	.225	.0050	.150	.012	.09	.009	.27
4	.020	.300	.0067	.200	.016	.12	.012	.36
5	.025	.375	.0083	.250	.020	.15	.015	.45
6	.030	.450	.0100	.300	.024	.18	.018	.54
7	.035	.525	.0117	.350	.028	.21	.021	.63
8	.040	.600	.0134	.400	.032	.24	.024	.72
9	.045	.675	.0150	.450	.036	.27	.027	.81
10	.050	.750	.0167	.500	.040	.30	.030	.90
Condition			Servo and surface limits					
Normal functioning	Maximum servo-actuator travel = ±1.0 inch or ±15° of horizontal stabilizer		Maximum servo-actuator travel = ±1.0 inch or ±15° of horizontal stabilizer		Maximum servo-actuator travel = ±1.0 inch or ±7.5° of vertical stabilizer		Maximum servo-actuator travel = ±1.0 inch or ±15° of horizontal stabilizer	
Mal-functioning	0.1 inch or 1.5° of horizontal stabilizer		0.1 inch or 3° differential stabilizer		0.1 inch or 0.75° of vertical stabilizer		0.1 inch or 3° of differential stabilizer	

TABLE III.- BASIC DATA FOR THE LONGITUDINAL MANEUVERS

Flight[1]	Power	SAS gain setting[2]	M	$\bar{q}$, lb/sq ft	h_p, ft	α, deg	P, sec	$T_{1/2}$, sec	$\frac{\lvert a_n \rvert}{\lvert \alpha \rvert}$
1-2-7	On	0,4,8	1.14	396	38,000	7.8	1.78	1.51	12.24
1-3-8	On	1,0,8	1.88	703	46,700	3.0	1.20	1.15	27.39
1-5-10	Off	0,4,8	1.72	536	48,900	9.4	1.36	2.40	23.39
1-9-17	On	0,4,8	1.63	288	59,600	7.9	2.00	4.90	9.09
1-9-17	On	0,4,8	2.00	299	67,400	8.2	2.05	∞	9.69
1-9-17	Off	4,4,8	2.93	864	61,100	3.3	1.05	------	-------
1-9-17	Off	0,4,8	1.82	432	55,500	2.2	1.55	2.58	20.60
1-9-17	Off	0,4,8	1.73	545	48,500	2.6	1.40	1.88	24.86
1-9-17	Off	0,4,8	1.42	525	41,000	4.6	1.40	1.32	27.58
1-10-19	On	0,4,8	1.75	318	60,400	7.9	1.85	3.72	10.60
1-12-23	On	0,4,8	2.50	285	77,500	3.3	2.45	8.25	8.48
1-12-23	On	0,4,8	2.99	372	79,500	2.5	2.30	7.10	11.35
1-12-23	Off	0,2,2	2.31	504	62,300	9.6	1.60	3.25	18.89
1-12-23	Off	0,4,8	1.44	363	49,600	6.2	1.70	1.72	19.80
1-12-23	Off	0,4,8	1.19	280	46,800	8.8	1.96	1.60	15.60
1-15-28	On	4,4,8	1.49	435	47,200	8.1	1.00	------	-------
1-15-28	On	4,4,8	1.82	670	46,500	2.6	.95	------	-------
1-16-29	On	0,4,8	1.48	393	48,900	3.8	1.76	2.90	12.02
1-16-29	On	0,4,8	1.67	538	47,400	3.9	1.46	1.98	22.40
1-17-30	Off	4,4,8	1.78	438	54,400	10.7	.40	------	-------
1-17-30	On	4,4,8	1.55	438	48,600	9.8	.38	------	-------
1-19-32	On	0,4,8	1.46	416	47,100	8.6	1.58	3.04	15.55
1-19-32	Off	0,4,8	1.36	367	46,700	3.6	1.66	2.28	19.68
1-20-35	On	0,4,8	1.60	554	45,100	9.7	1.40	2.00	-------
2-1-3	On	2,4,8	1.17	276	46,300	5.2	2.10	0.75	7.54
2-1-3	On	2,4,8	1.87	604	49,800	2.2	1.21	1.00	23.56
2-1-3	Off	2,4,8	.96	185	46,500	4.4	2.11	.75	10.31
2-2-6	On	2,4,8	1.03	288	40,300	8.7	1.60	1.32	12.10
2-2-6	On	2,0,8	1.05	283	41,500	8.4	1.90	1.38	9.59
2-2-6	On	2,0,8	1.45	362	49,900	10.0	1.40	.92	18.09
2-2-6	Off	2,0,8	1.66	467	50,200	1.3	1.30	.78	23.18
2-2-6	Off	0,0,8	.88	247	37,700	5.2	2.26	1.24	15.91
2-4-11	On	0,4,8	1.73	304	60,700	11.1	1.90	2.10	9.95
2-6-13	Off	0,0,0	.80	280	30,400	4.0	2.76	2.22	14.32
2-6-13	Off	0,0,0	.64	237	23,400	5.0	2.20	------	-------
2-8-16	On	0,4,8	1.12	336	40,600	8.9	1.94	1.80	9.87
2-8-16	On	0,4,8	1.18	290	45,700	7.8	2.10	2.35	9.19
2-8-16	On	0,4,8	1.41	318	51,400	2.3	1.93	2.80	10.16
2-8-16	On	0,4,8	1.57	417	50,100	5.6	1.63	2.55	12.81
2-9-18	On	0,2,8	1.28	269	50,700	.2	2.15	3.00	8.99
2-9-18	On	0,2,8	1.42	322	51,300	3.1	1.94	2.95	10.73

[1]First digit indicates airplane by number (X-15-1 or X-15-2), second indicates free-flight number of the particular airplane, third indicates total airborne X-15/B-52 flights for that airplane.

[2]Numbers given for SAS gain setting are damper-gain knob positions of the pitch, roll, and yaw, respectively. The yar gain is connected to the roll-damper gain knob. Damper gains corresponding to various knob settings are shown in table II.

TABLE IV.- BASIC DATA FOR THE LATERAL-DIRECTIONAL MANEUVERS

Flight[1]	Power	SAS gain setting[2]	M	$\bar{q}$, lb/sq ft	h_p, ft	α, deg	P, sec	$T_{1/2}$, sec	$\frac{\lvert r \rvert}{\lvert \beta \rvert}$
1-2-7	On	0,4,8	1.81	247	50,300	8.2	2.28	3.40	2.47
1-3-8	On	4,0,8	1.75	596	47,200	3.5	1.40	------	------
1-3-8	On	4,0,8	1.85	656	47,500	3.6	1.45	------	------
1-3-8	On	1,0,1	1.95	752	46,900	2.2	1.60	------	------
1-5-10	On	4,0,0	1.71	327	58,800	15.3	1.40	1.78	1.04
1-5-10	On	4,0,8	2.04	537	56,200	.4	2.00	------	------
1-5-10	Off	0,0,0	.84	204	39,100	4.0	2.40	------	------
1-6-11	On	4,0,0	1.72	309	60,200	12.0	1.76	2.30	1.64
1-6-11	Off	4,0,0	1.96	450	57,900	9.3	1.70	------	2.30
1-7-12	On	4,4,8	2.07	238	73,400	6.0	2.60	2.60	2.37
1-7-12	Off	4,4,8	2.05	797	64,400	3.5	2.00	1.14	3.64
1-7-12	Off	4,4,0	2.44	669	58,700	8.4	1.90	4.60	3.19
1-9-17	Off	4,0,0	2.78	818	60,100	3.3	1.95	------	3.25
1-9-17	Off	4,4,8	2.71	803	59,300	3.4	1.60	1.54	3.78
1-9-17	Off	4,0,0	2.29	606	39,100	9.8	2.00	------	------
1-10-19	Off	4,0,0	2.15	774	50,500	4.3	1.58	2.05	3.75
1-10-19	Off	4,0,0	2.88	676	47,500	3.8	1.48	1.87	4.29
1-12-23	On	4,2,2	2.26	478	38,200	6.2	1.70	------	------
1-14-27	On	4,0,0	1.94	623	50,600	3.2	1.68	2.30	3.66
1-16-29	On	4,0,0	1.76	584	47,900	1.6	1.55	2.35	3.64
1-16-29	On	4,0,0	1.82	628	47,700	1.4	1.57	1.93	3.73
1-18-31	On	4,4,8	2.20	298	46,000	10.9	2.20	------	------
1-18-31	On	4,4,8	1.61	518	46,700	3.7	1.60	------	------
1-18-31	On	4,4,8	1.70	562	47,200	3.3	1.60	------	------
1-19-32	On	4,0,0	1.38	442	43,700	4.5	1.68	2.77	3.26
1-19-32	On	4,0,8	1.45	412	47,100	7.8	1.30	------	------
1-20-35	On	4,0,0	1.87	866	42,500	7.4	1.31	1.30	4.37
1-21-36	Off	4,4,8	2.38	650	58,300	5.3	1.80	.95	3.65
2-1-3	On	2,4,8	1.17	276	46,300	5.1	1.20	0.77	------
2-1-3	On	2,4,8	1.24	286	48,100	4.7	1.80	.93	3.07
2-1-3	On	2,4,8	1.79	533	50,500	2.2	1.51	.75	3.62
2-1-3	On	2,4,8	1.87	625	49,500	2.3	.91	.84	------
2-1-3	Off	2,4,8	.96	177	47,500	4.0	3.00	1.64	2.42
2-1-3	Off	2,4,8	.96	185	46,500	4.6	1.00	.40	------
2-2-6	On	2,0,8	1.06	270	42,700	8.6	2.90	------	------
2-2-6	On	2,4,8	1.06	257	43,900	8.8	2.90	------	------
2-2-6	On	2,0,8	1.21	193	55,300	4.4	2.37	------	------
2-2-6	On	2,4,8	1.29	215	55,800	4.9	1.58	------	------
2-2-6	On	2,0,8	1.37	244	55,400	4.8	2.40	------	------
2-2-6	On	2,0,8	1.47	340	51,700	6.1	1.26	------	------
2-2-6	On	2,4,8	1.70	300	60,500	2.2	2.00	------	------
2-2-6	Off	2,0,8	1.73	444	52,900	.5	1.64	------	------
2-2-6	Off	2,0,8	1.70	451	51,900	.9	1.64	------	------
2-2-6	Off	2,0,8	1.03	246	43,500	3.9	2.37	------	------
2-2-6	Off	2,0,8	.89	231	38,800	3.5	1.97	------	------
2-2-6	Off	2,0,0	.85	245	35,800	5.3	2.18	1.64	2.23
2-5-12	On	2,0,0	1.32	296	50,100	3.6	2.00	3.15	3.36
2-5-12	On	4,0,0	2.53	497	45,500	8.6	1.40	------	------
2-6-13	Off	0,0,0	.80	268	31,400	4.1	2.38	------	------
2-6-13	Off	0,0,0	.79	290	28,900	4.3	2.43	------	------
2-6-13	Off	0,0,0	.66	245	24,100	4.8	2.23	------	------
2-7-15	On	0,0,0	1.11	342	39,700	9.6	2.00	1.87	3.17
2-7-15	On	0,0,0	1.18	288	45,815	7.0	2.20	2.30	2.45

[1]First digit indicates airplane by number (X-15-1 or X-15-2), second indicates free-flight number of the particular airplane, third indicates total airborne X-15/B-52 flights for that airplane.

[2]Numbers given for SAS gain setting are damper-gain knob positions of the pitch, roll, and yaw, respectively. The yar gain is connected to the roll-damper gain knob. Damper gains corresponding to various knob settings are shown in table II.

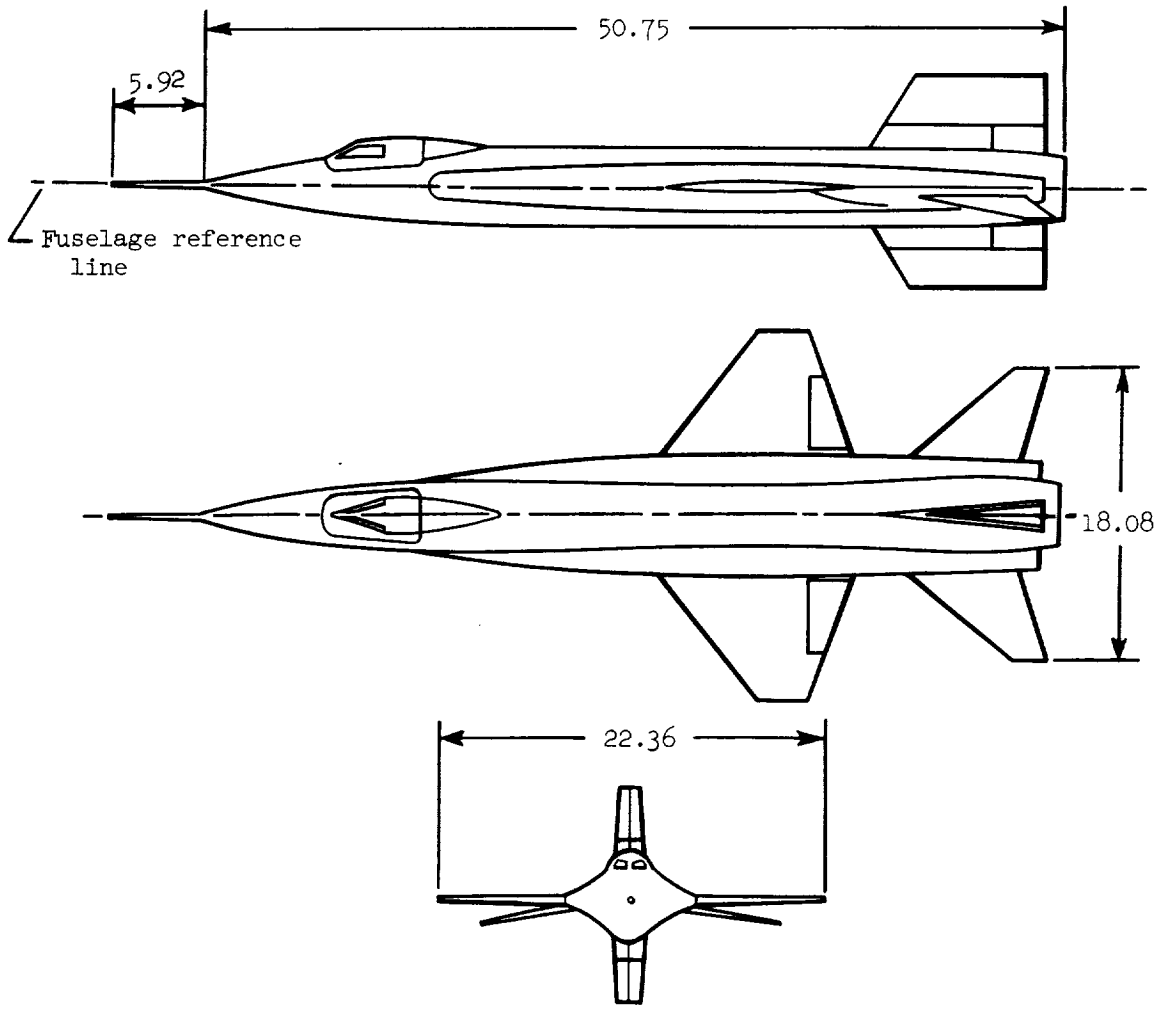

Figure 1.- Three-view drawing of the X-15 airplane. All dimensions in feet.

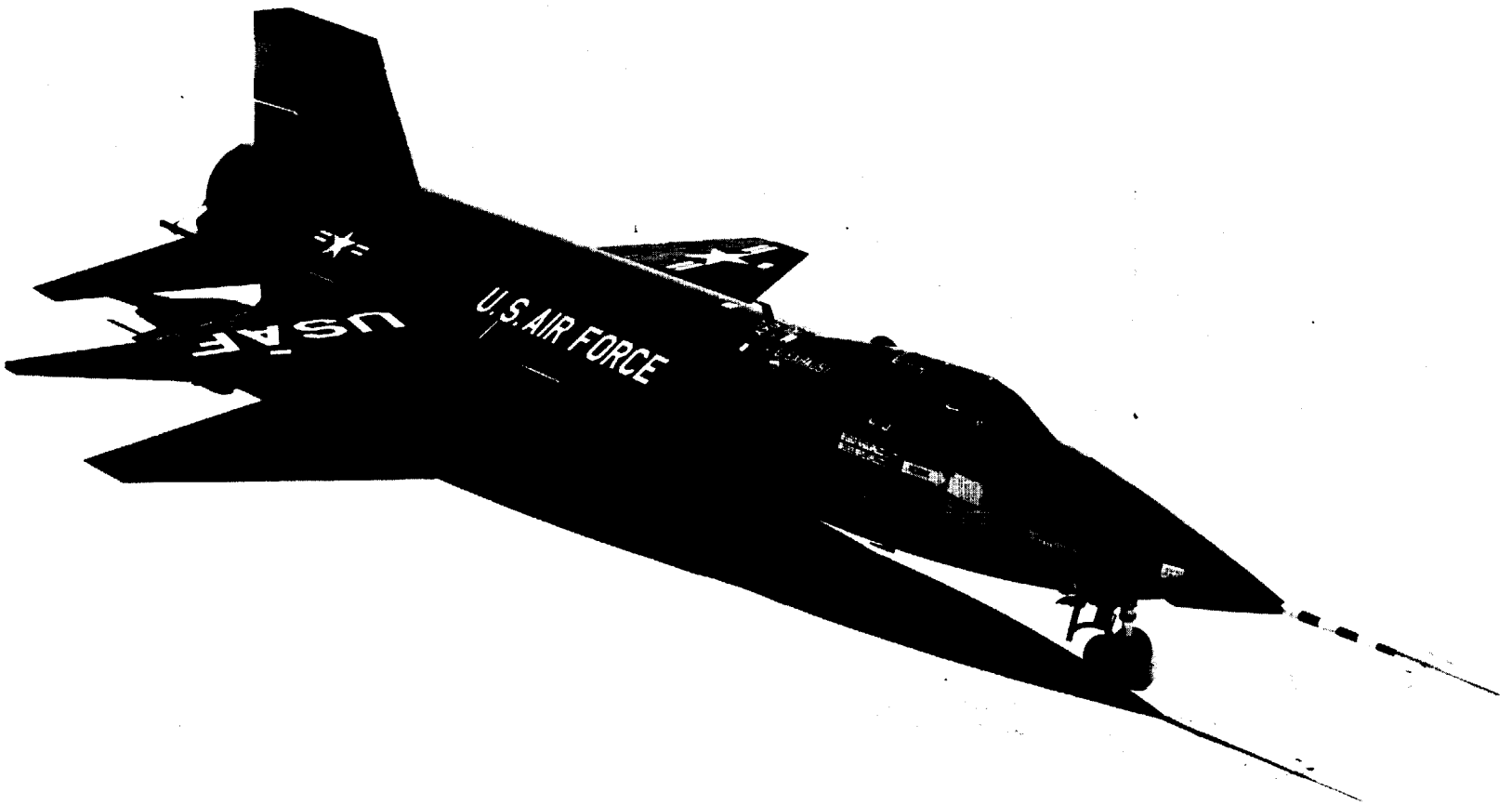

Figure 2.- Photograph of the X-15 airplane. E-5250

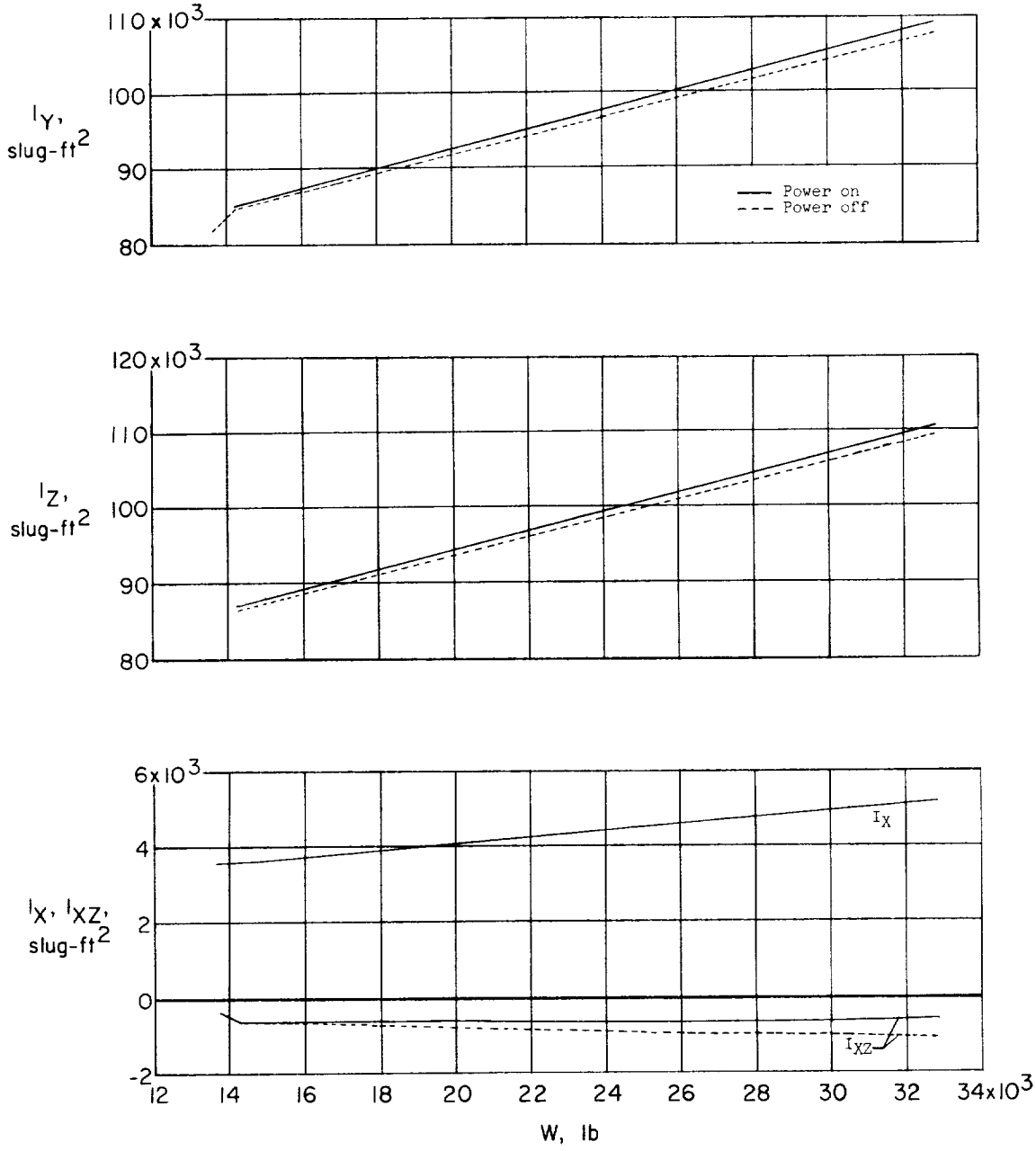

Figure 3.- Variation of the moments of inertia with airplane weight about the body reference axes (based on manufacturer's estimates).

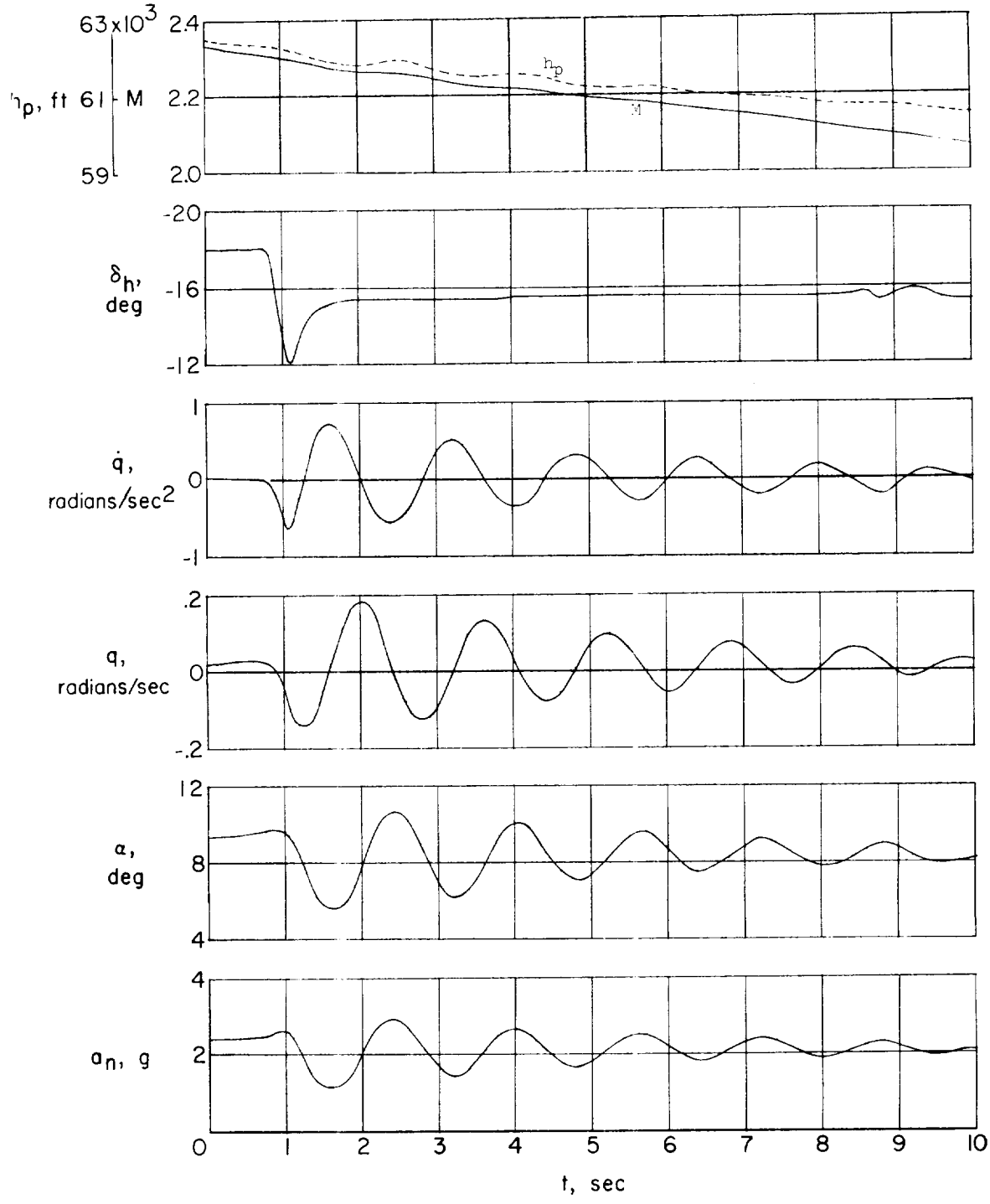

Figure 4.- Typical time histories of the longitudinal response characteristics resulting from an abrupt stabilizer input.

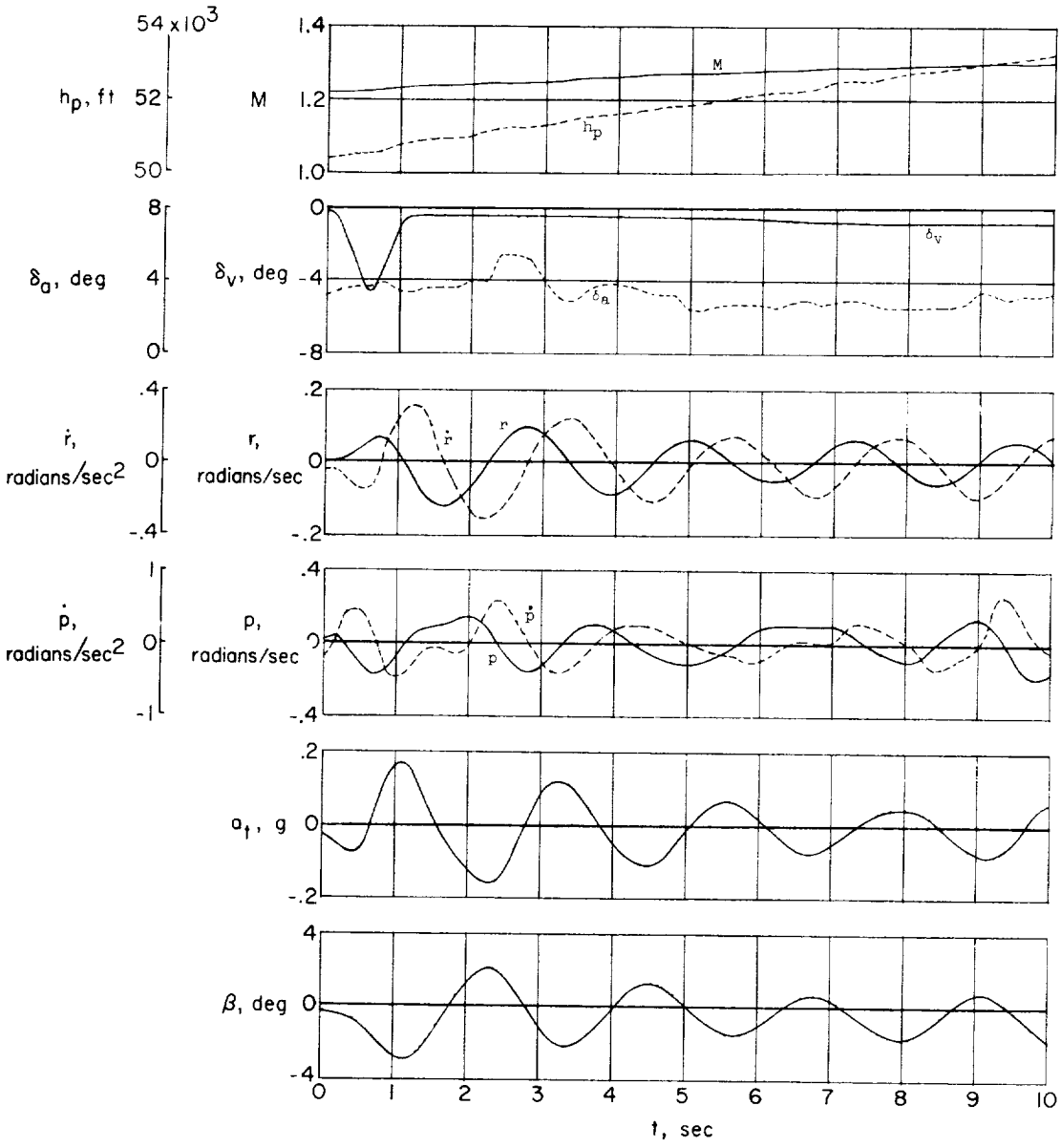

(a) Vertical-tail deflection (SAS off).

Figure 5.- Typical time histories of the lateral and directional response characteristics resulting from an abrupt vertical-tail deflection and aileron input.

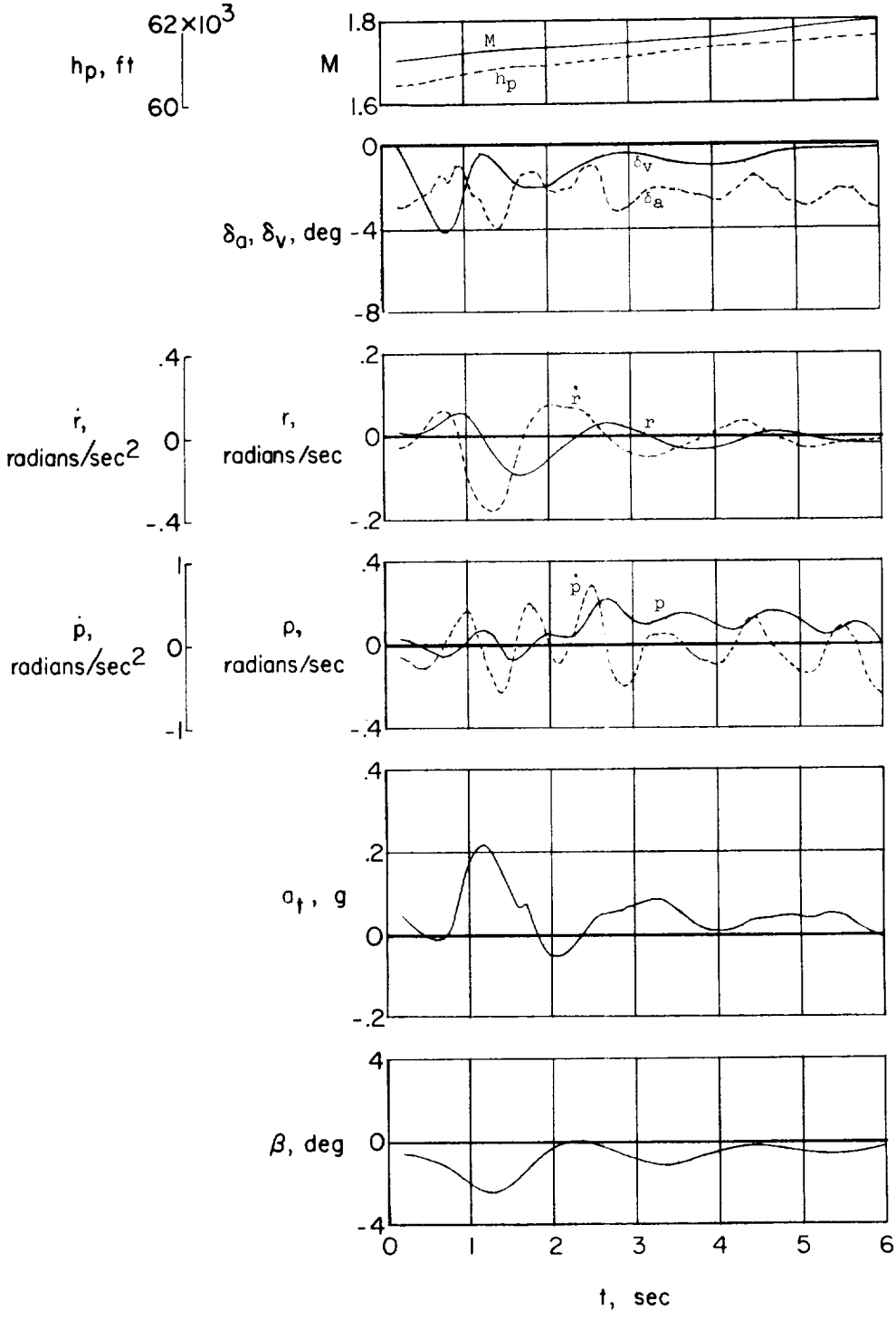

(b) Vertical-tail deflection (SAS on).

Figure 5.- Continued.

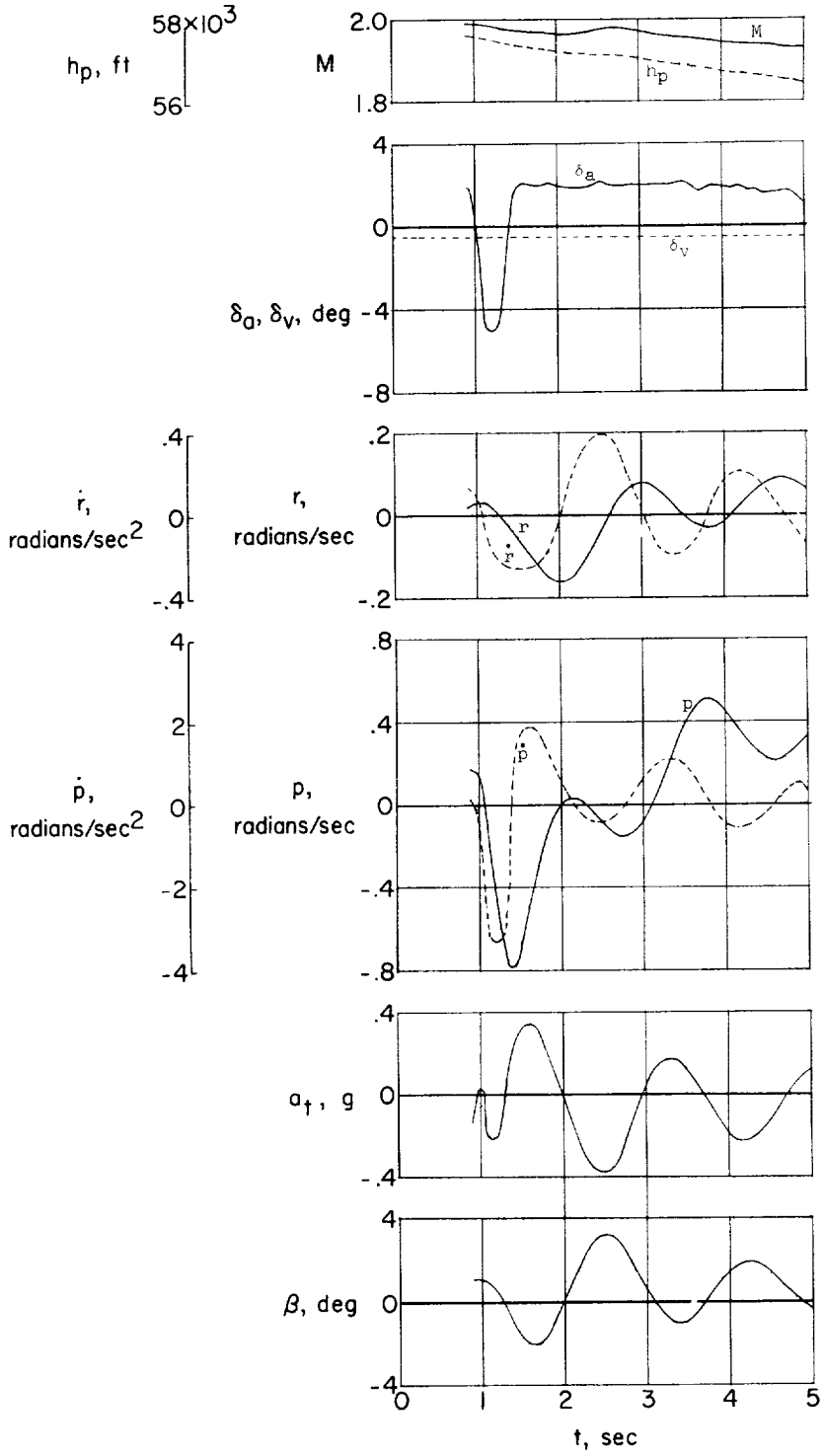

(c) Aileron deflection (SAS off).

Figure 5.- Continued.

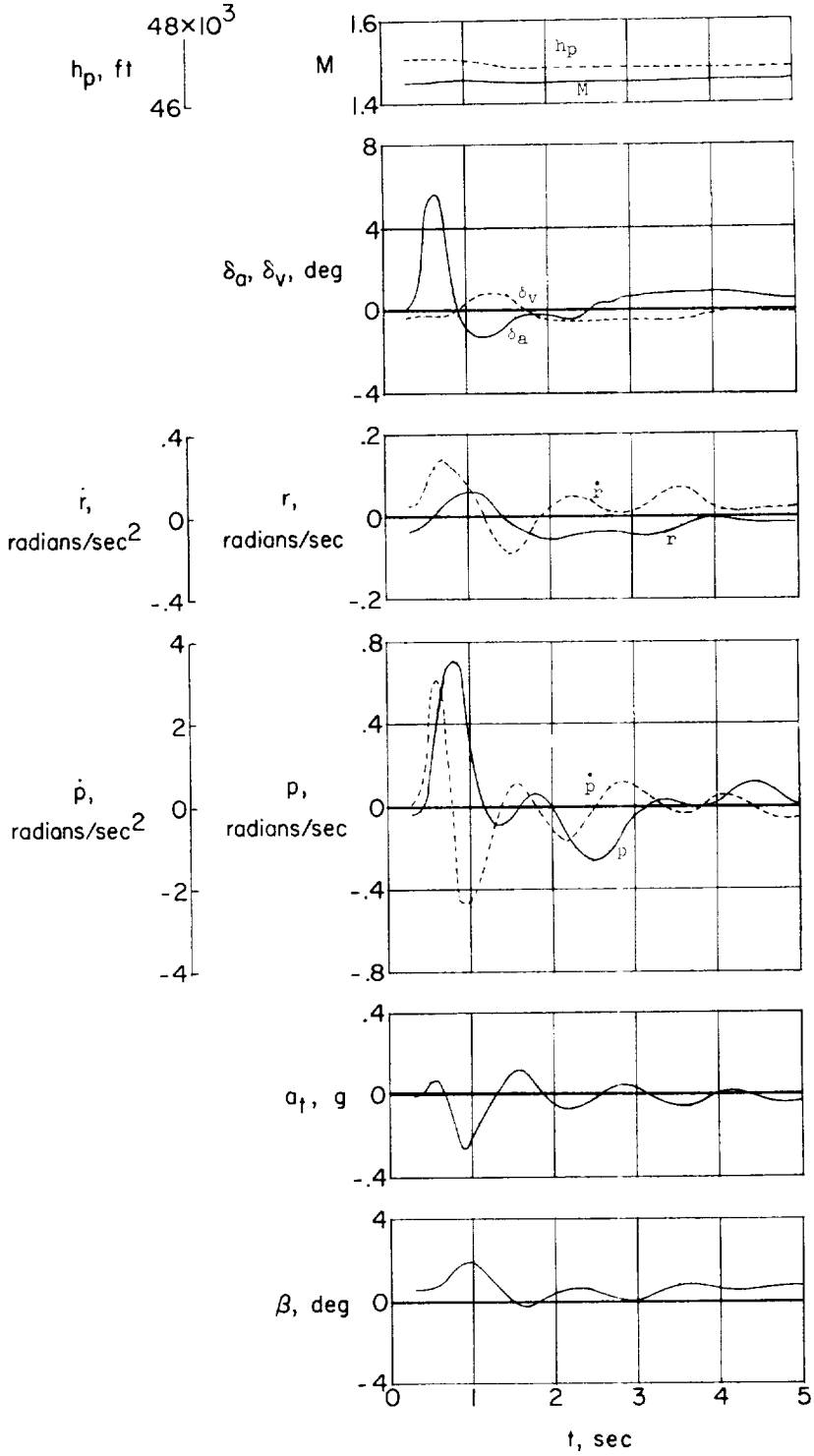

(d) Aileron deflection (SAS on).

Figure 5.- Concluded.

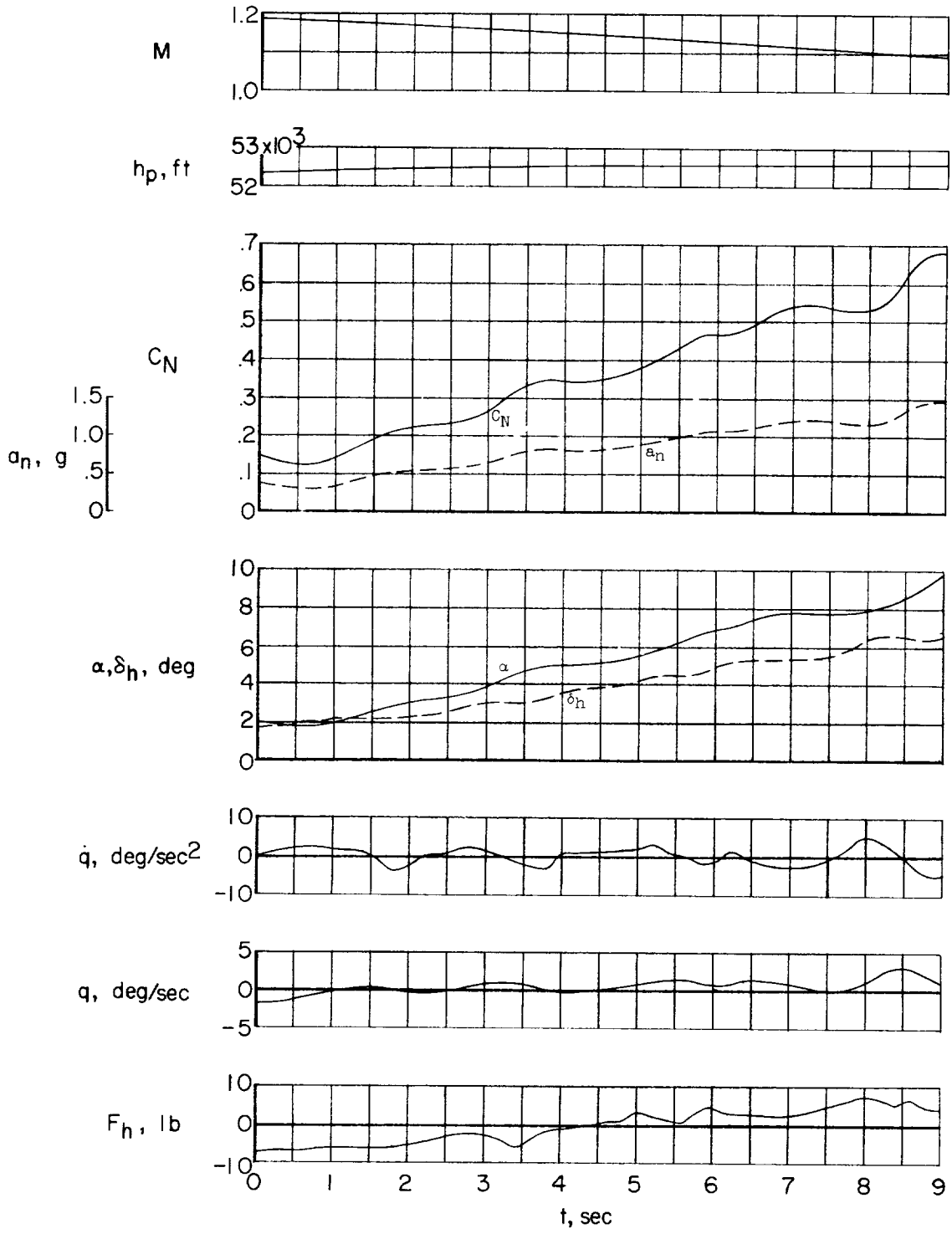

Figure 6.- Time history of a typical pull-up maneuver.

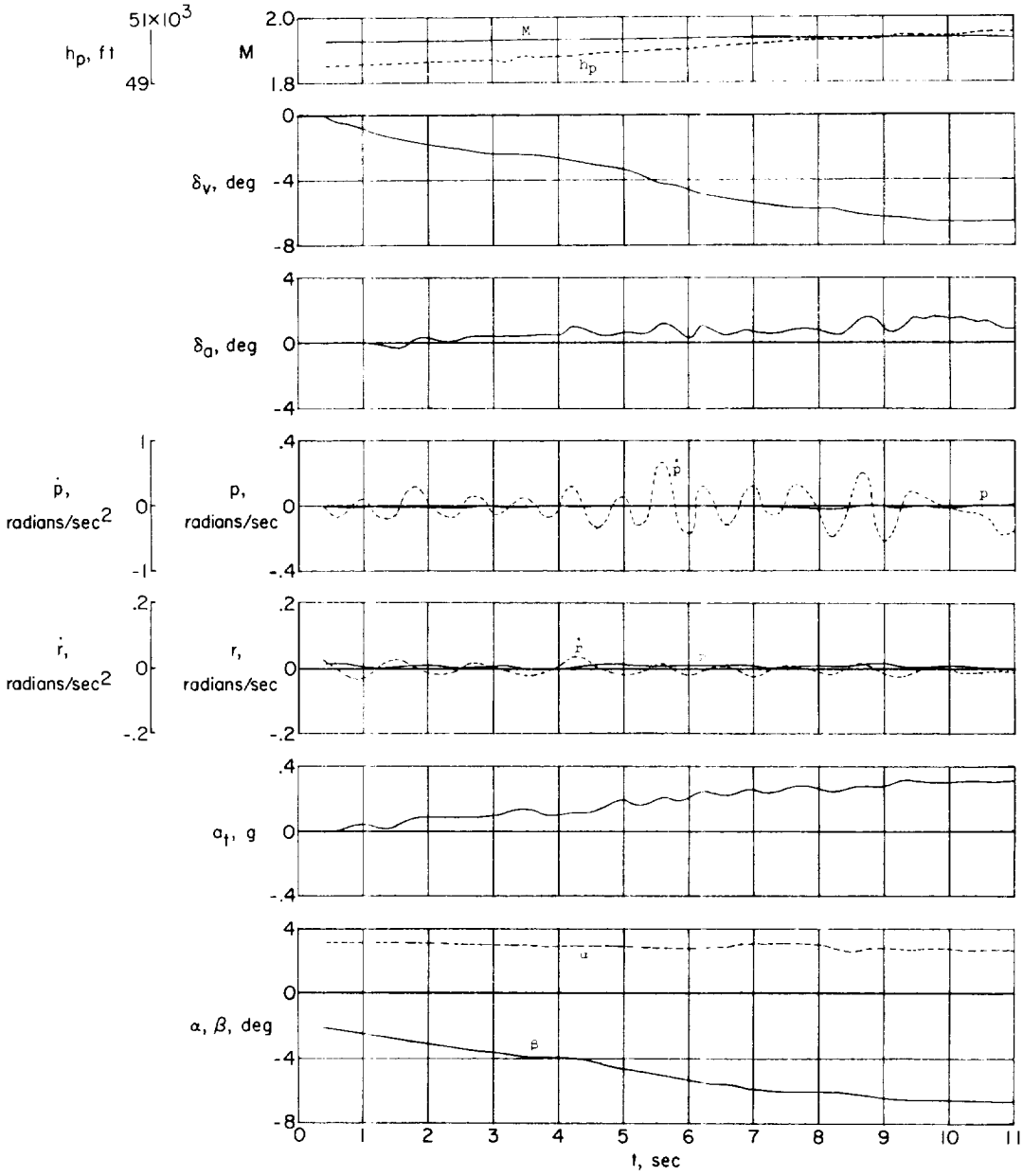

Figure 7.- Time history of a typical sideslip maneuver.

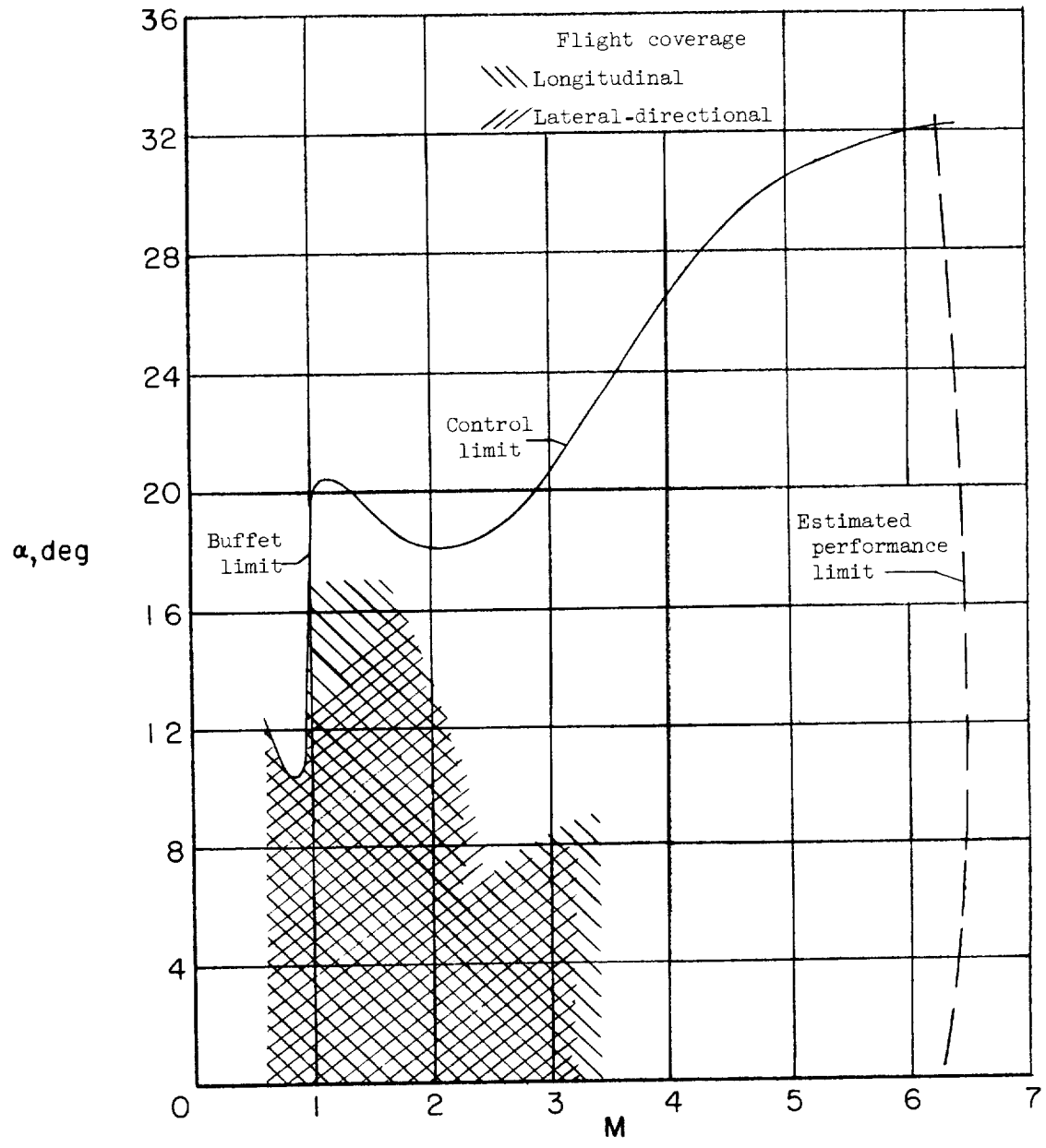

Figure 8.- Extent of flight coverage of X-15 stability and control derivatives.

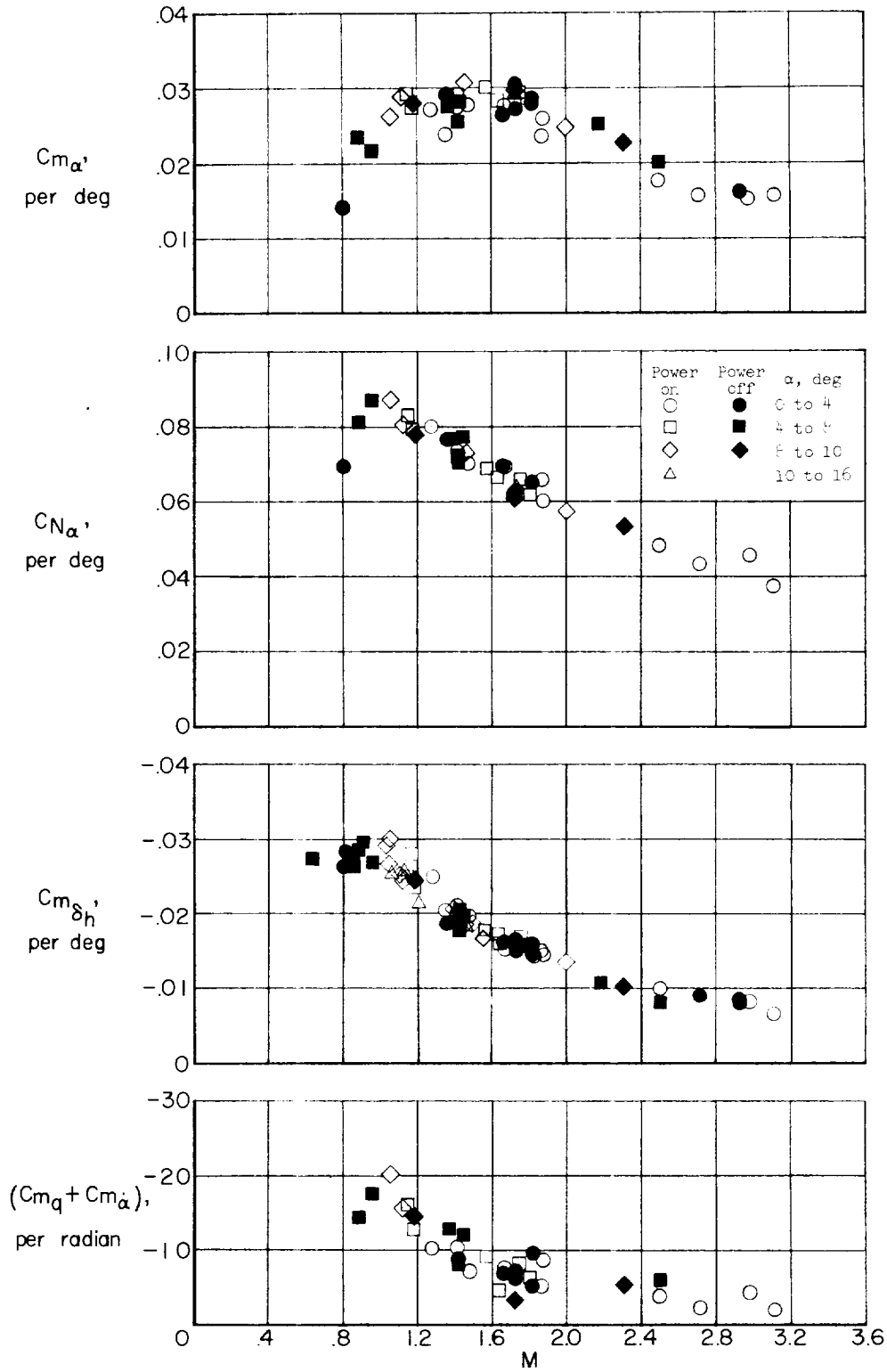

Figure 9.- Variation with Mach number of the longitudinal stability and control derivatives determined from flight data.

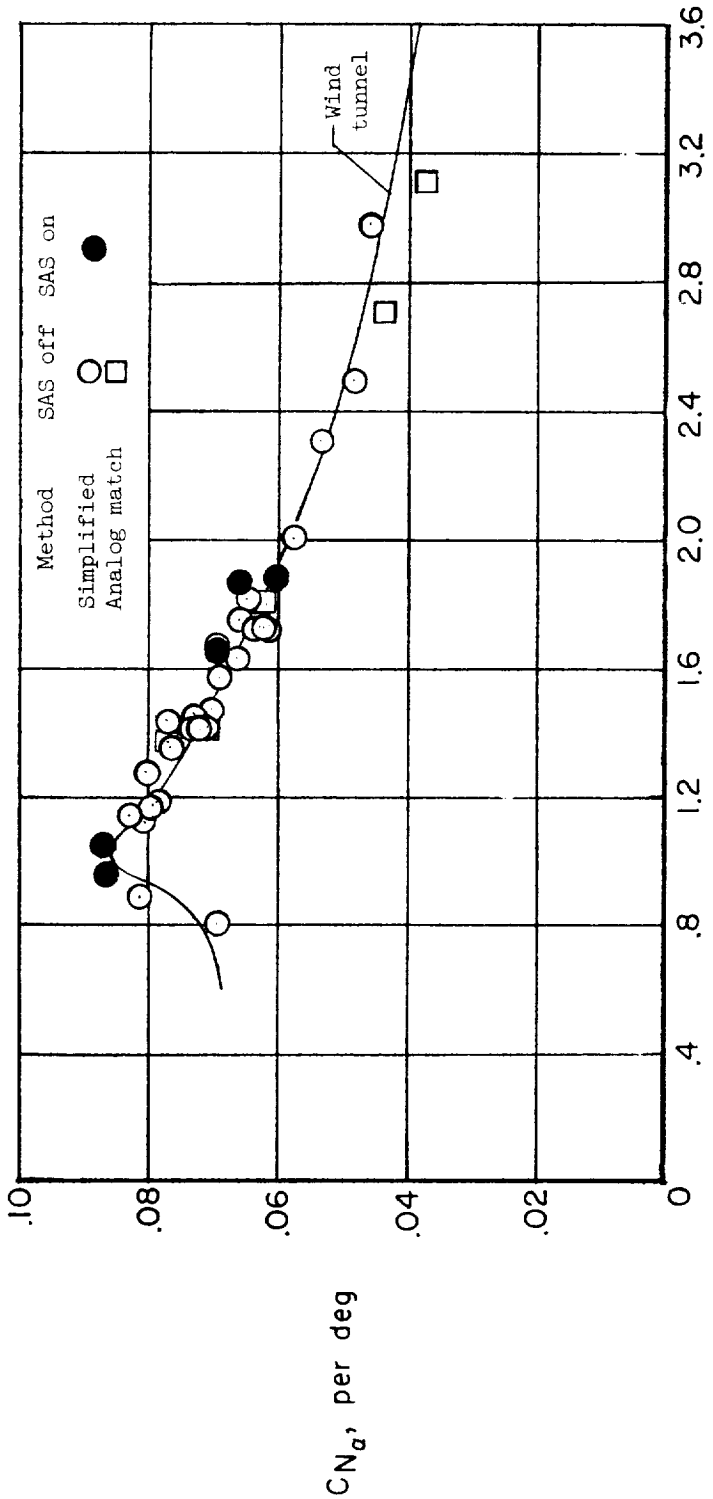

(a) Pulse maneuvers.

Figure 10.- Comparison of flight-determined normal-force-curve slope with wind-tunnel results.

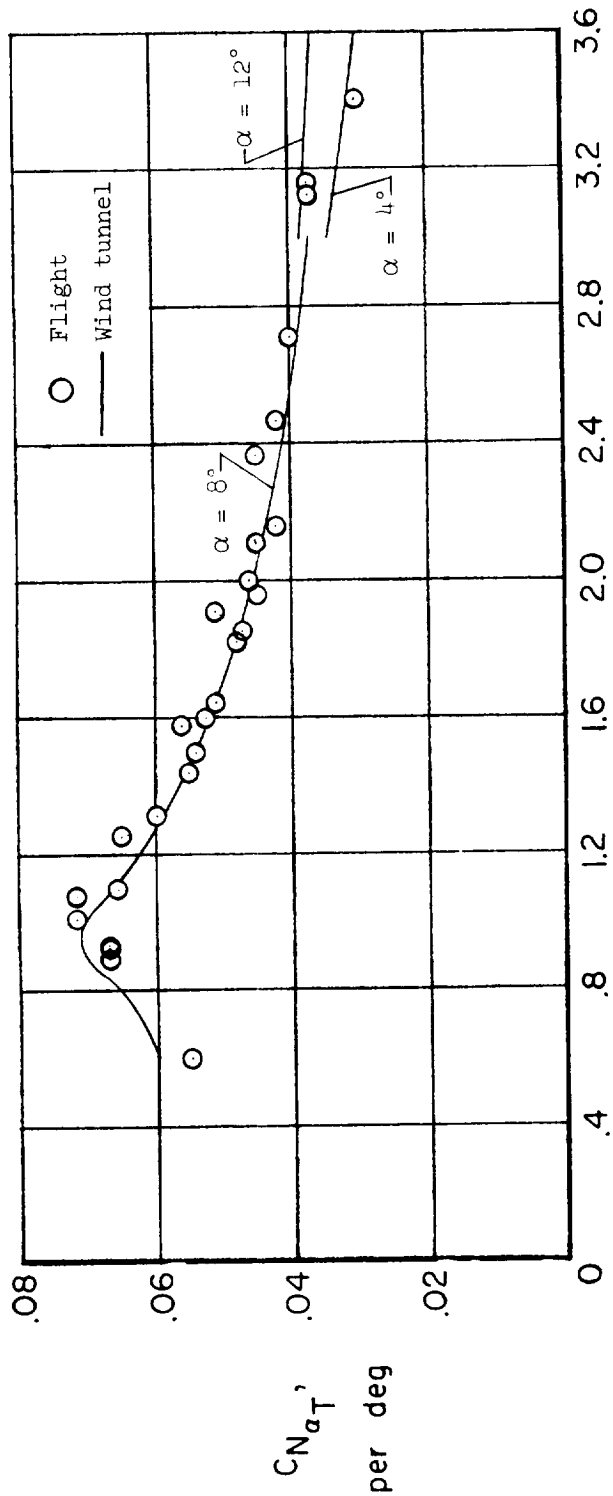

(b) Pull-up maneuver.

Figure 10.- Concluded.

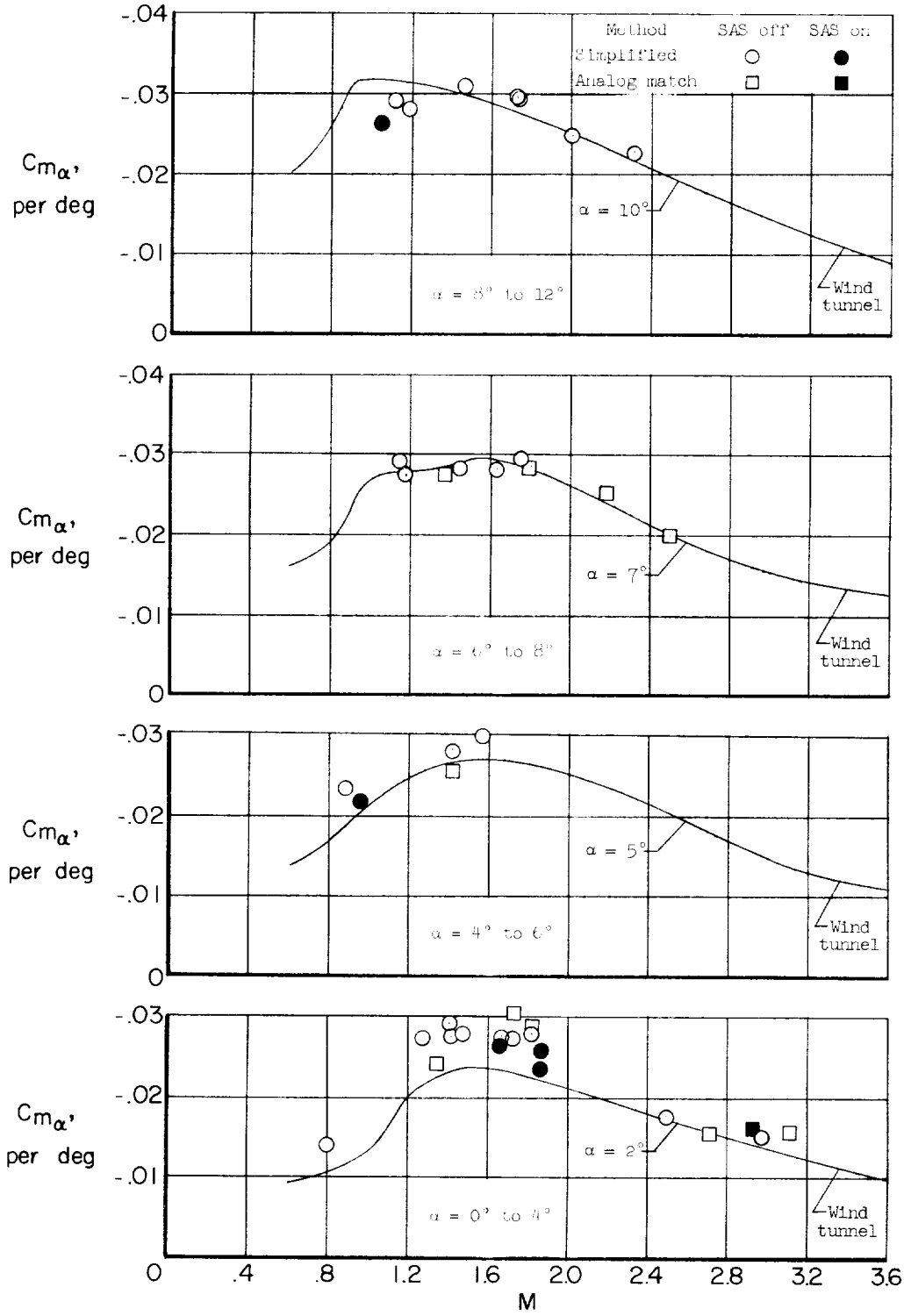

Figure 11.- Comparison of flight-determined longitudinal-stability derivatives with wind-tunnel results.

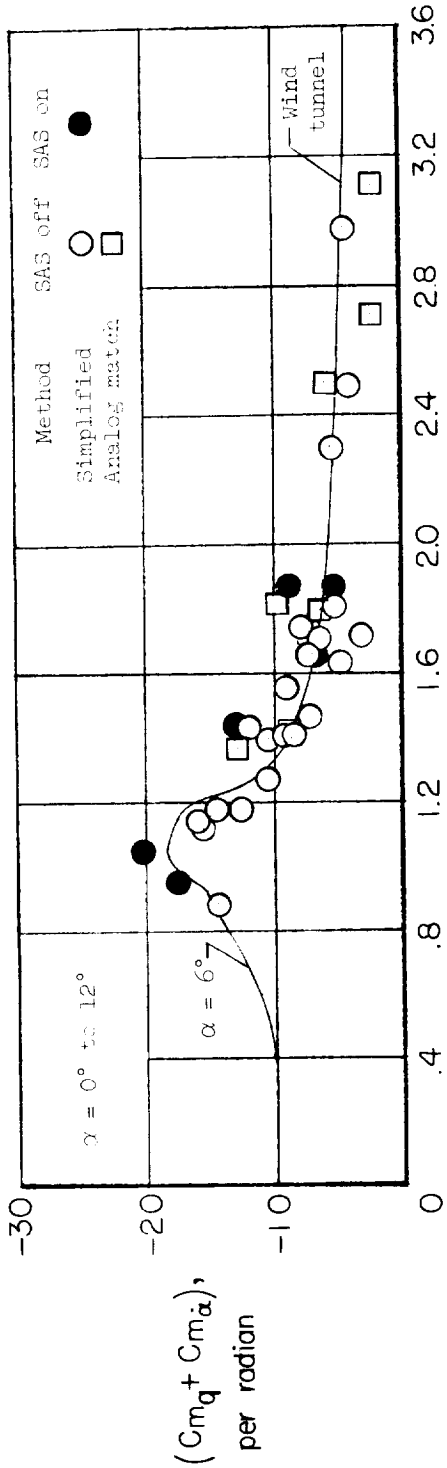

Figure 12.- Comparison of flight-determined pitch-damping derivatives with wind-tunnel data.

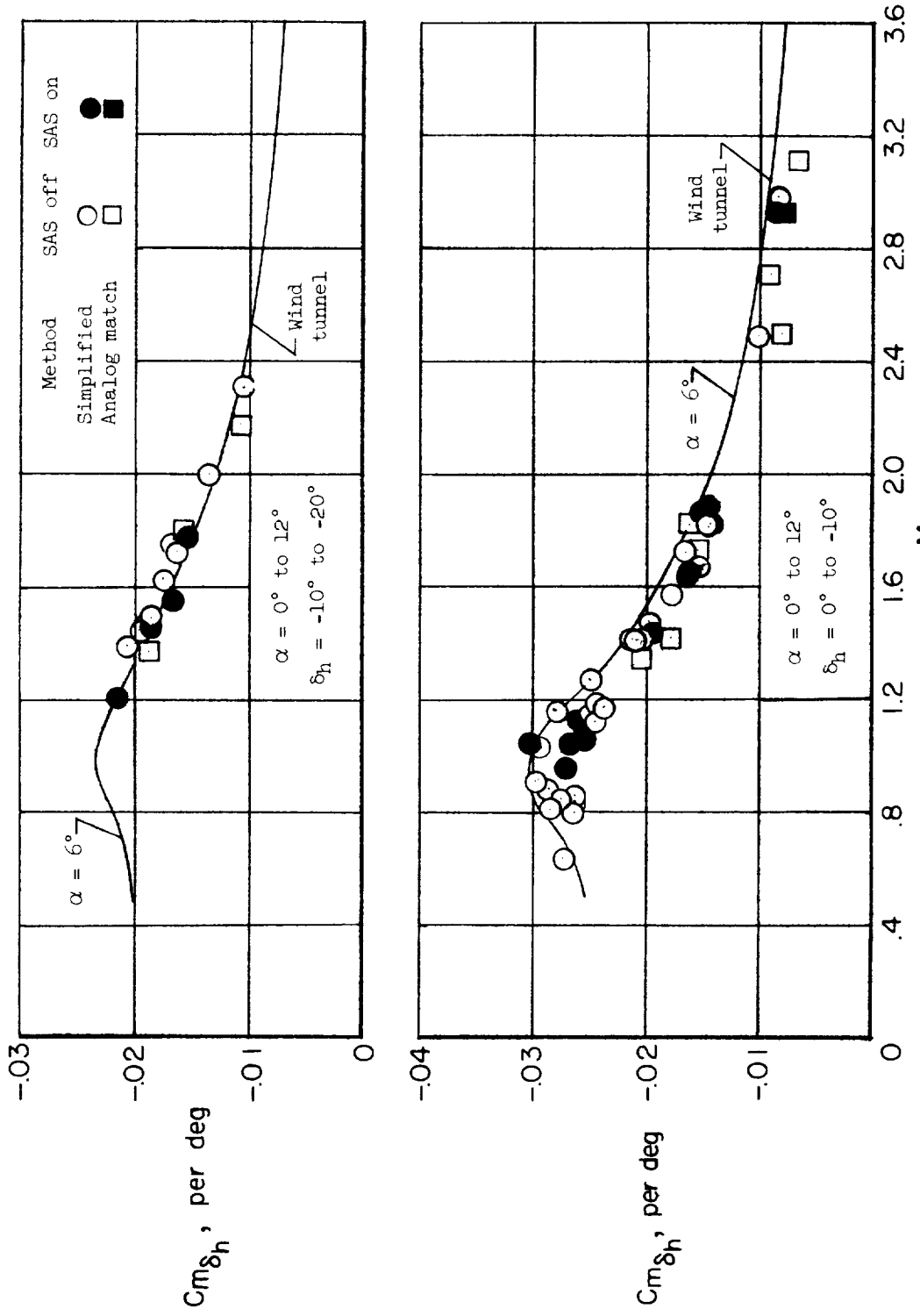

Figure 13.- Comparison of flight and wind-tunnel results used in obtaining horizontal-tail effectiveness.

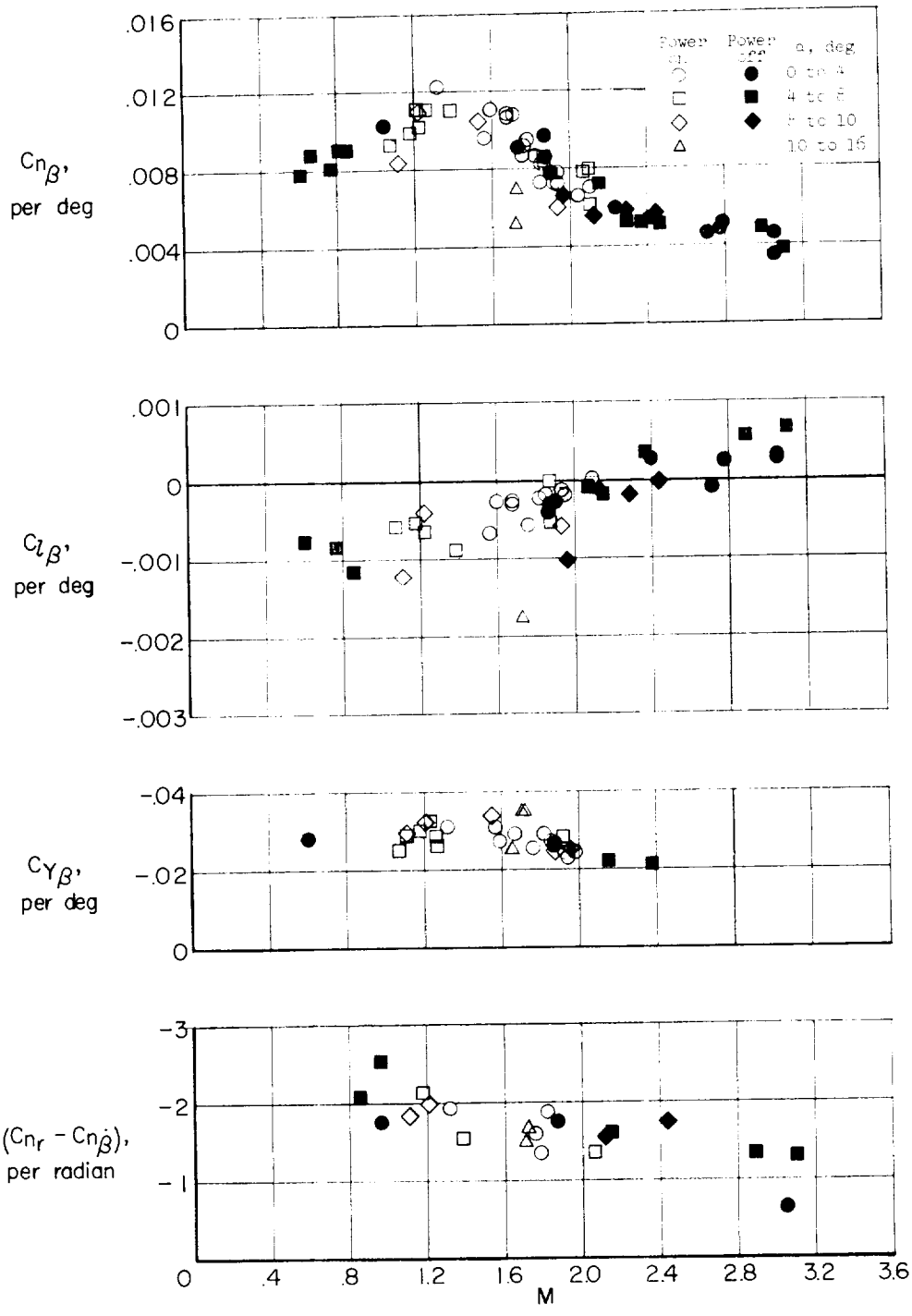

Figure 14.- Variation with Mach number of the flight-determined lateral-stability derivatives.

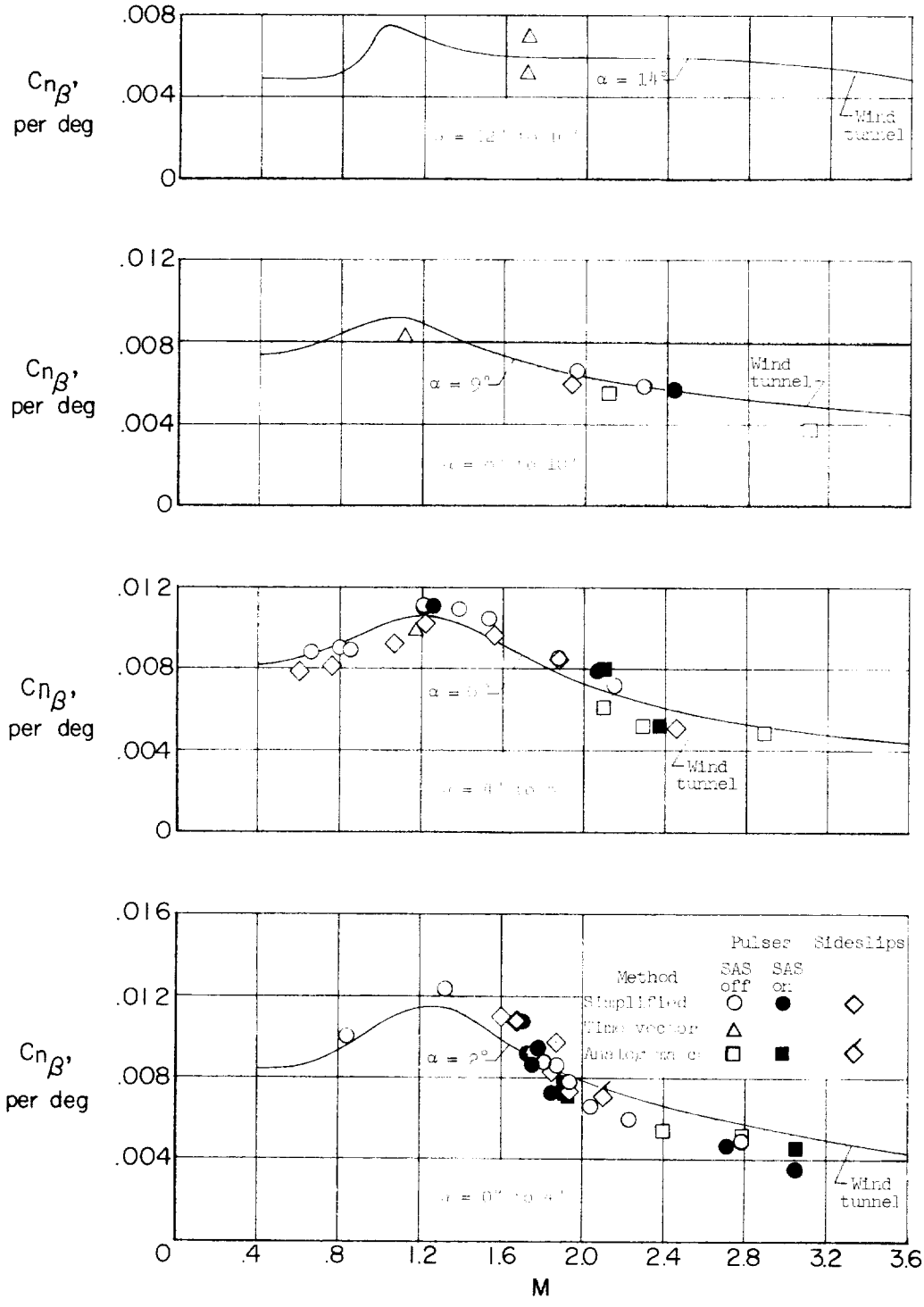

Figure 15.- Comparison of flight-determined directional-stability derivatives with wind-tunnel predictions.

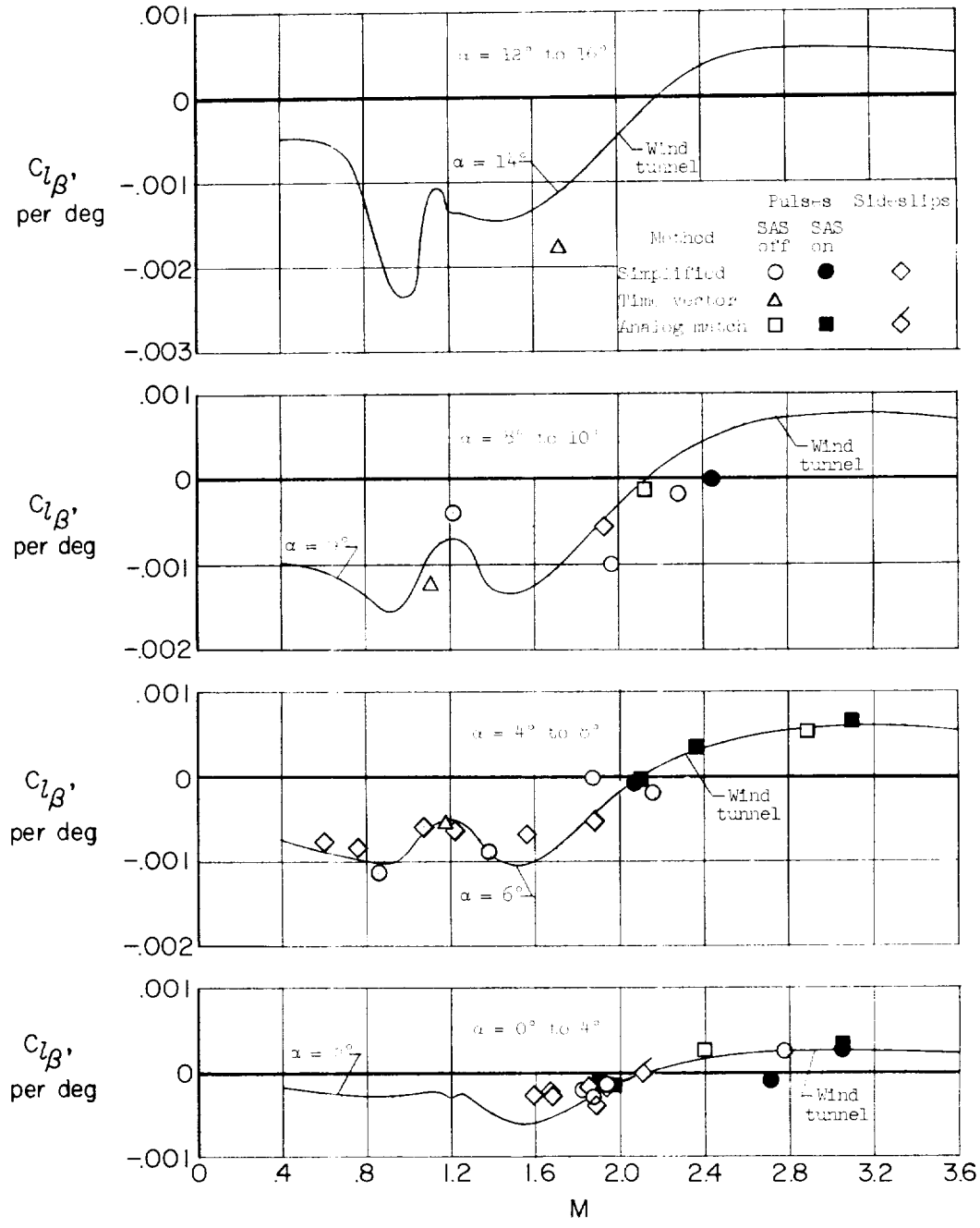

Figure 16.- Comparison of flight-determined effective-dihedral derivatives with wind-tunnel data.

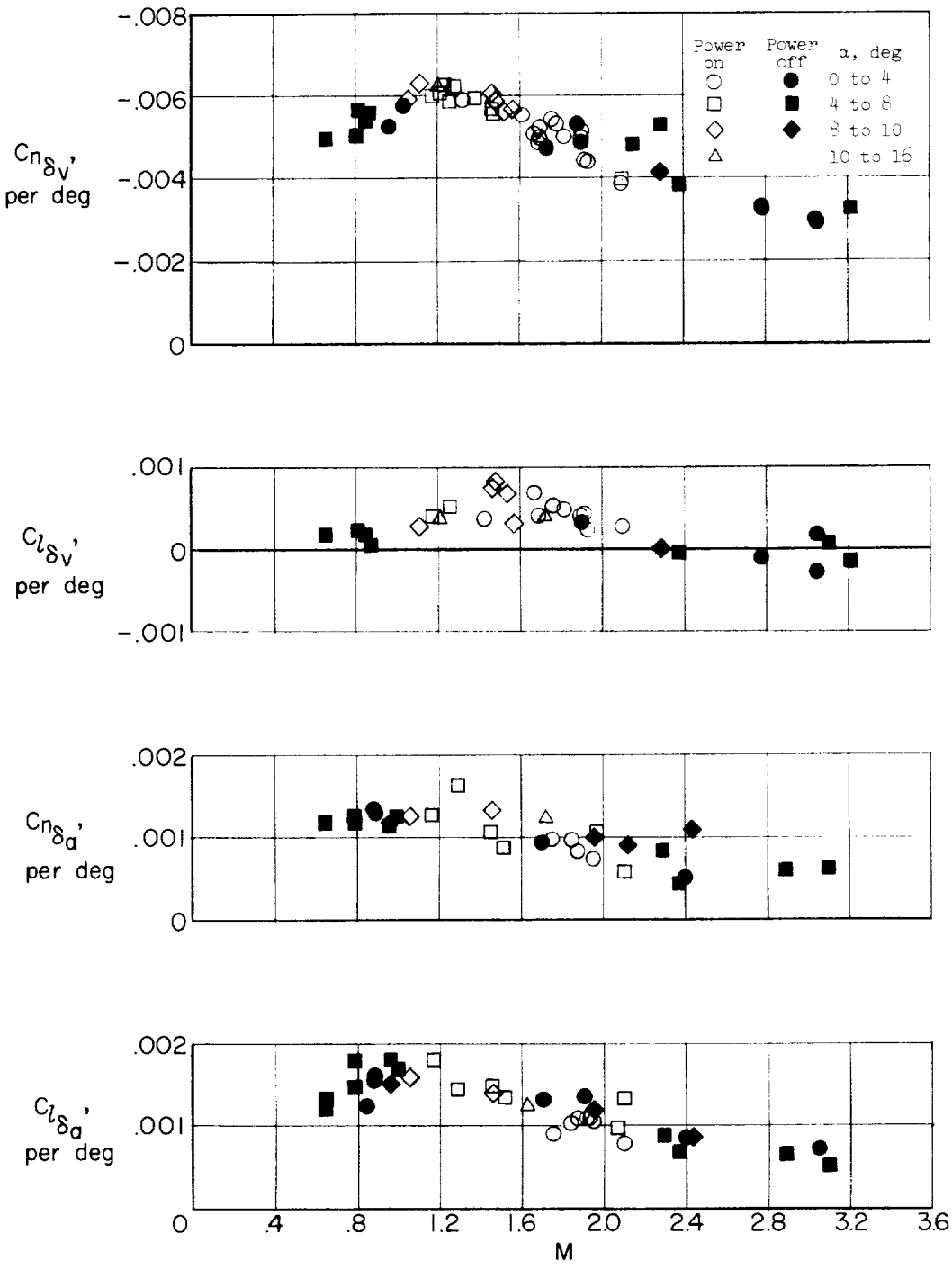

Figure 17.- Variation with Mach number of flight-determined lateral-control derivatives.

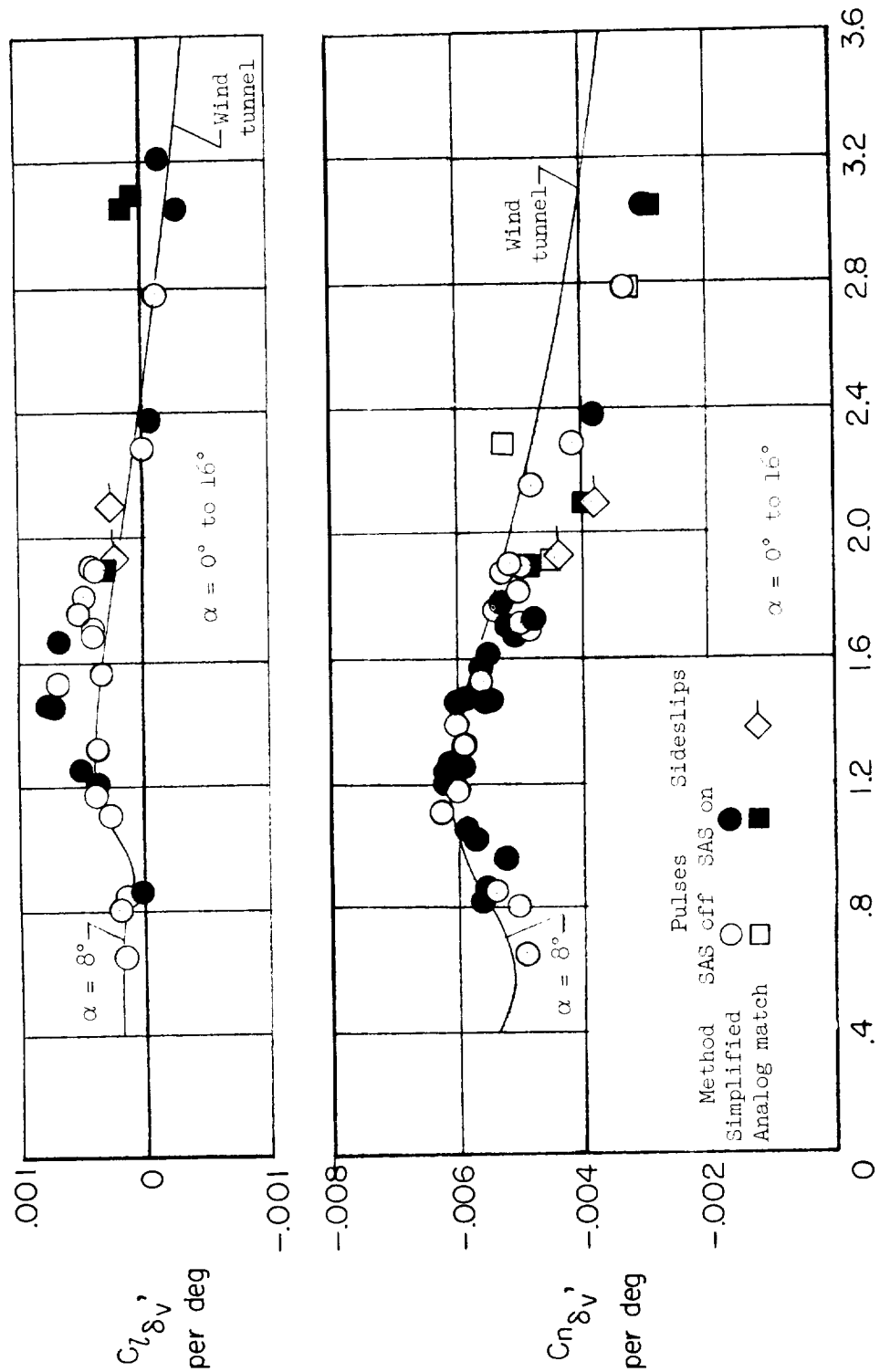

Figure 18.- Comparison of flight-determined directional-control derivatives with wind-tunnel predictions.

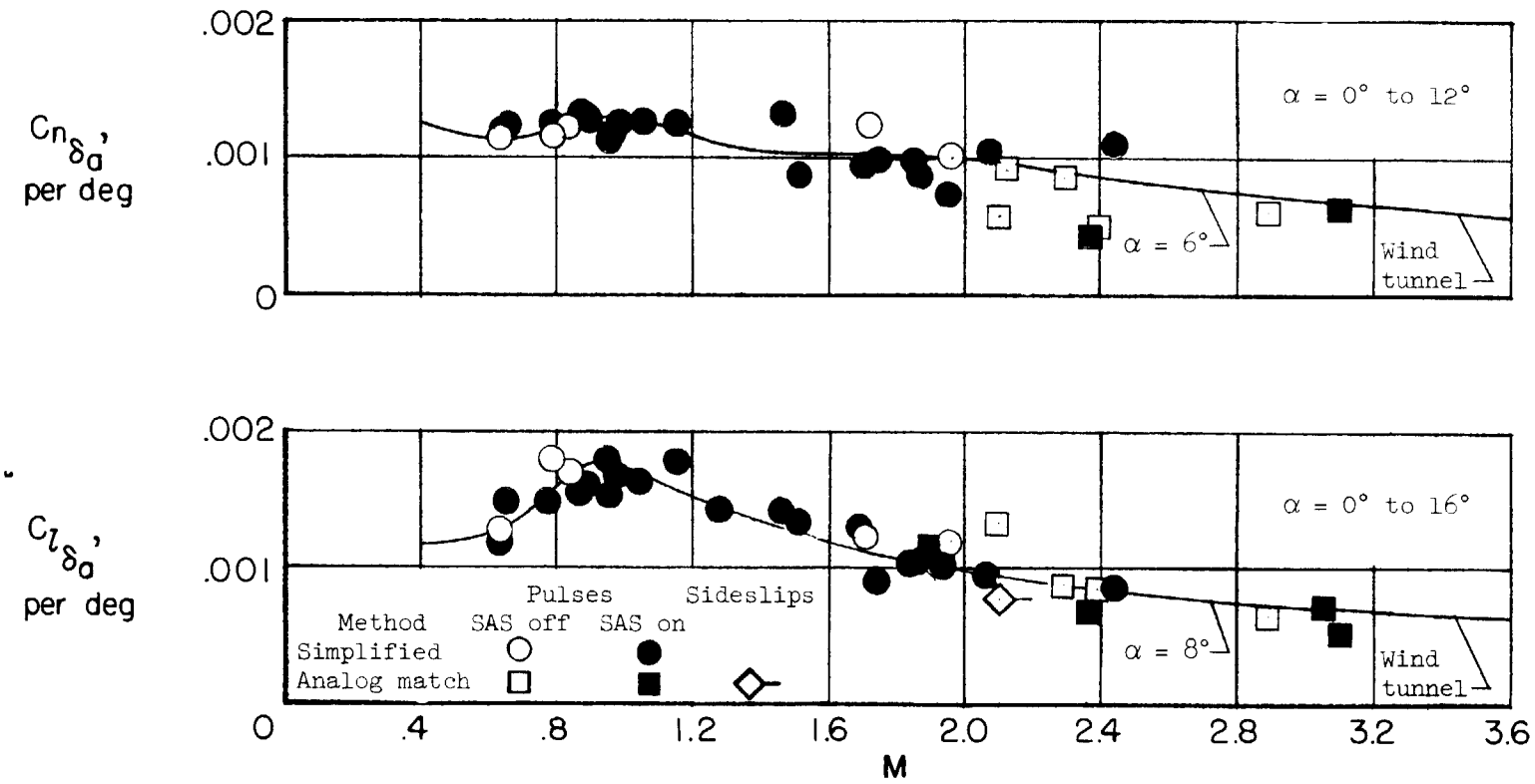

Figure 19.- Comparison of flight-determined roll-control derivatives with wind-tunnel predictions.

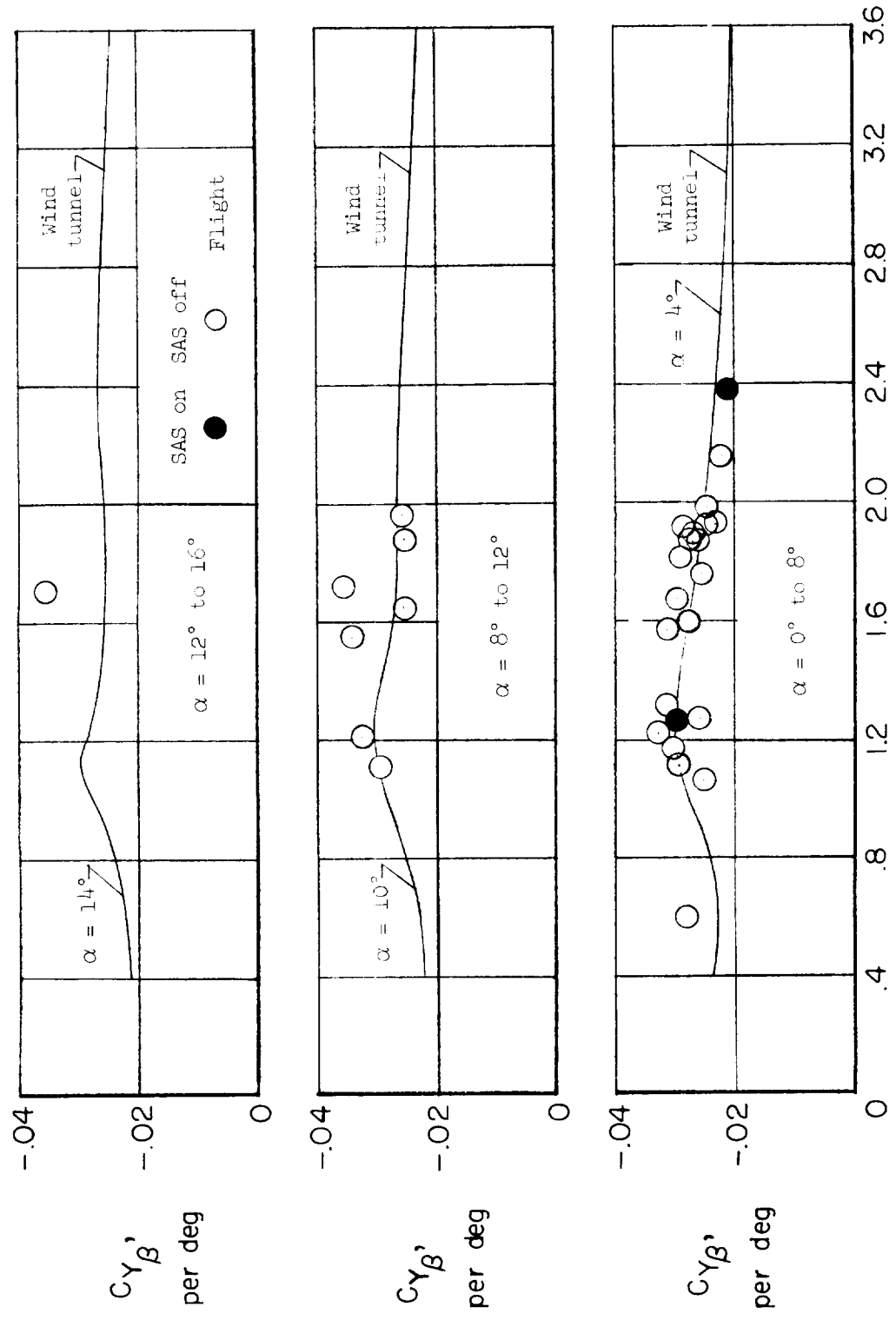

Figure 20.- Comparison of flight side-force derivatives, determined by the simplified method, with wind-tunnel data.

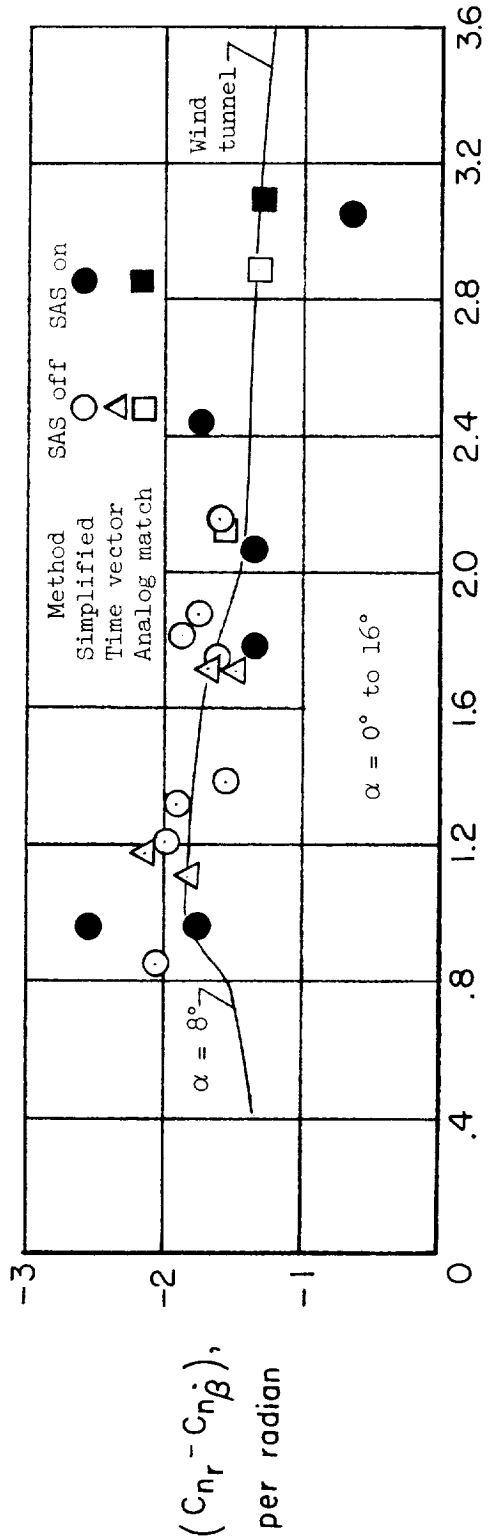

Figure 21.- Comparison of flight-determined damping-in-yaw derivatives with wind-tunnel data.

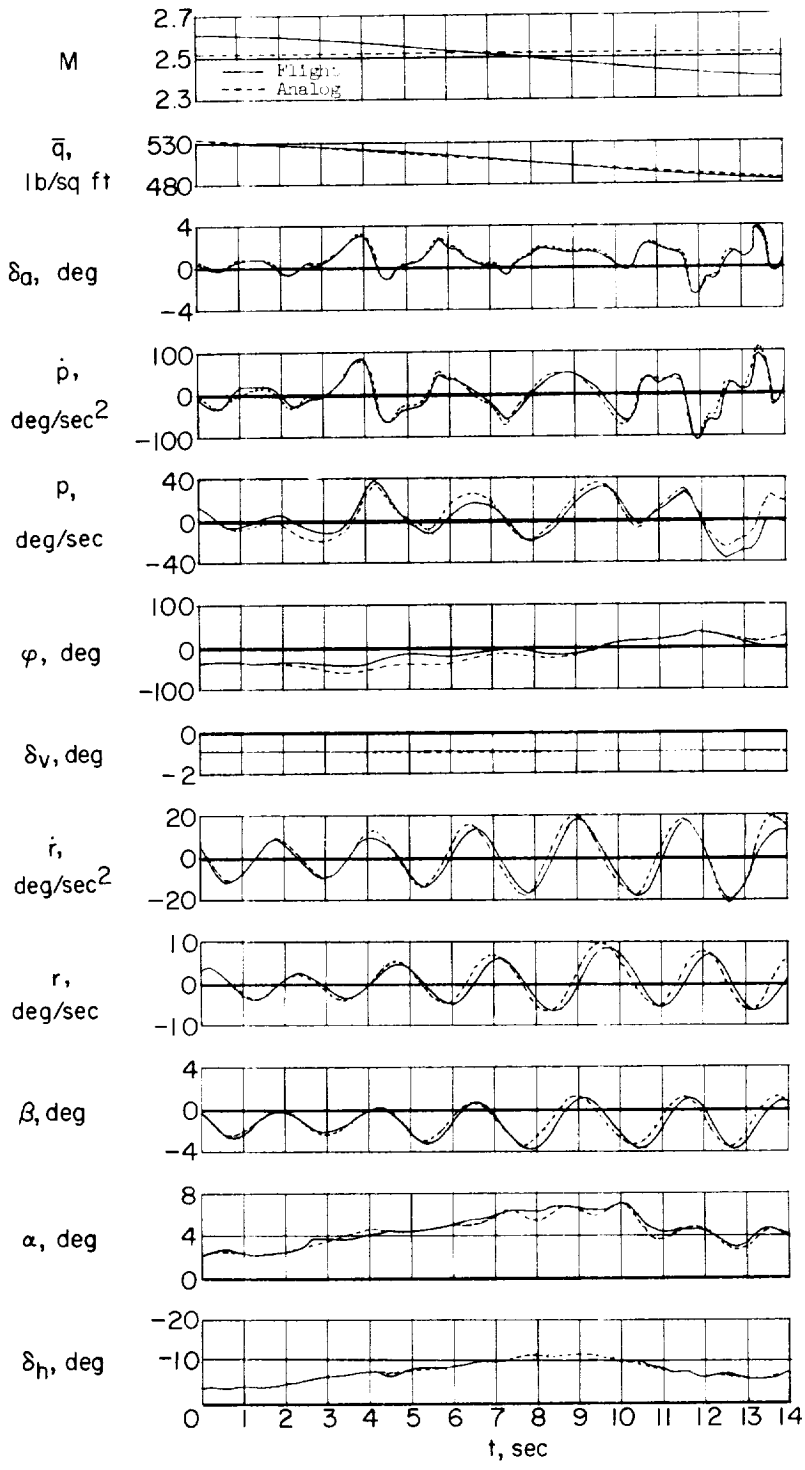

Figure 22.- Typical analog match of a yaw-roll divergence.

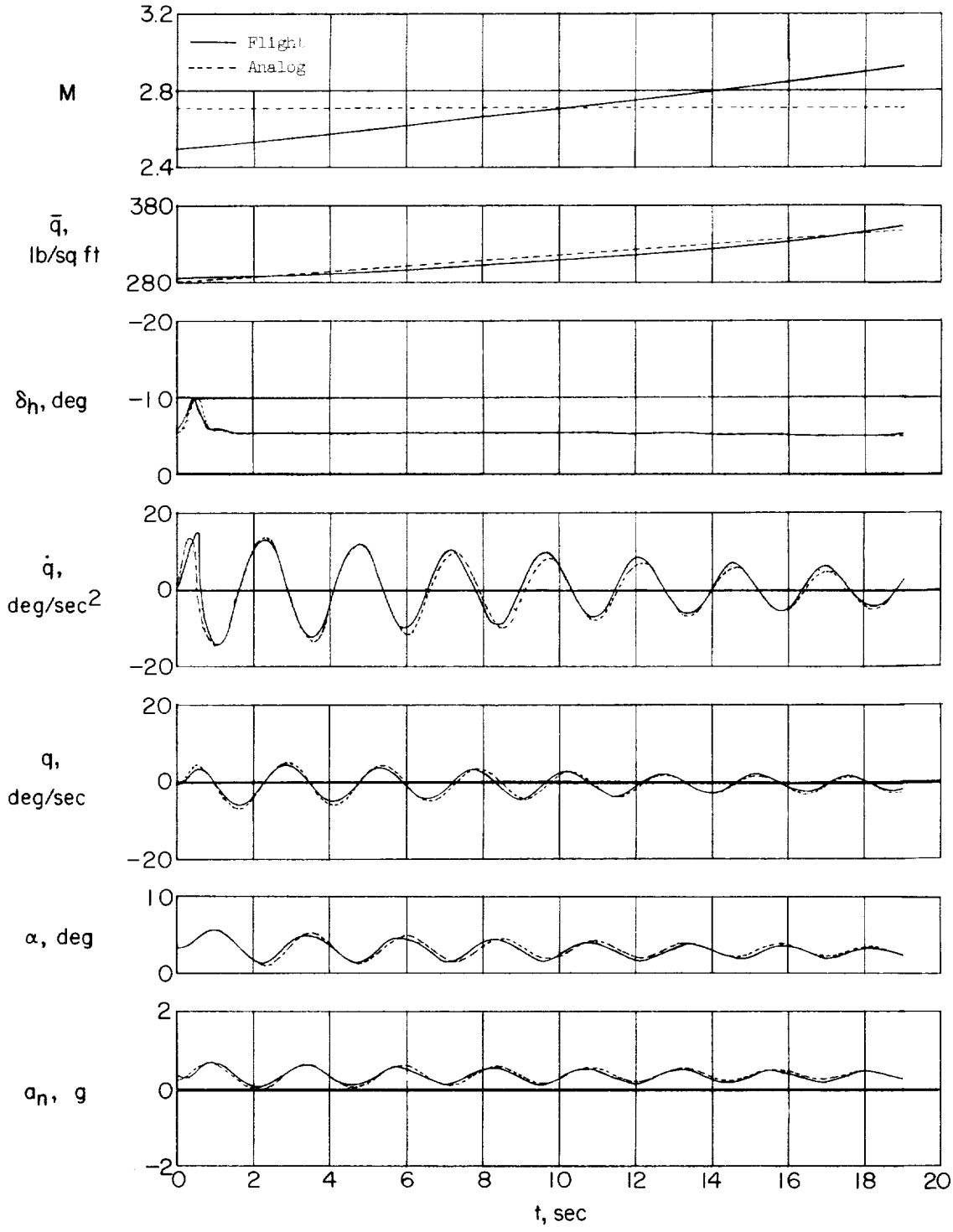

Figure 23.- Typical analog match of a horizontal-stabilizer pulse.

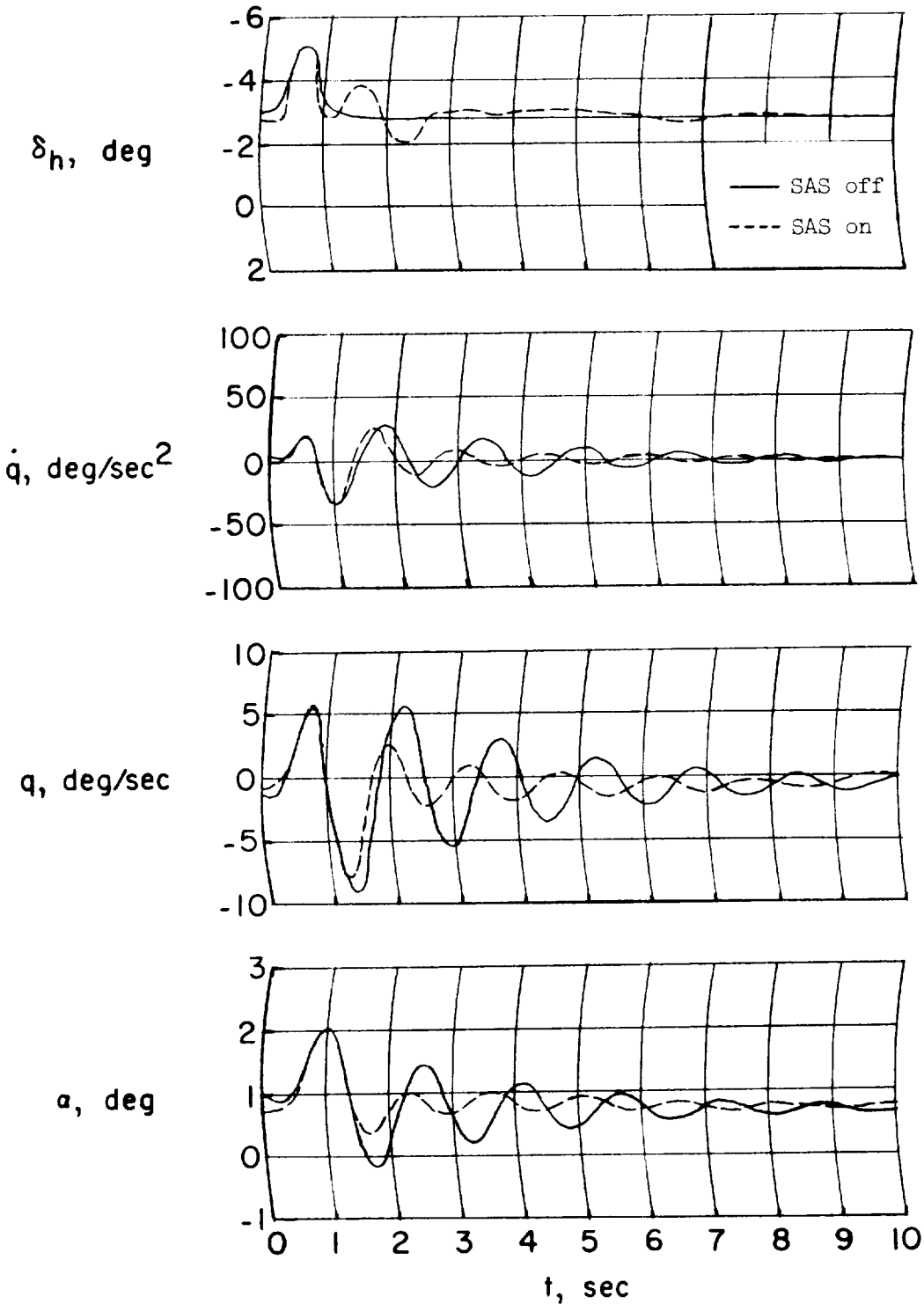

Figure 24.- Time histories of longitudinal pulses performed on the X-15 analog with the stability augmentation system engaged and disengaged.

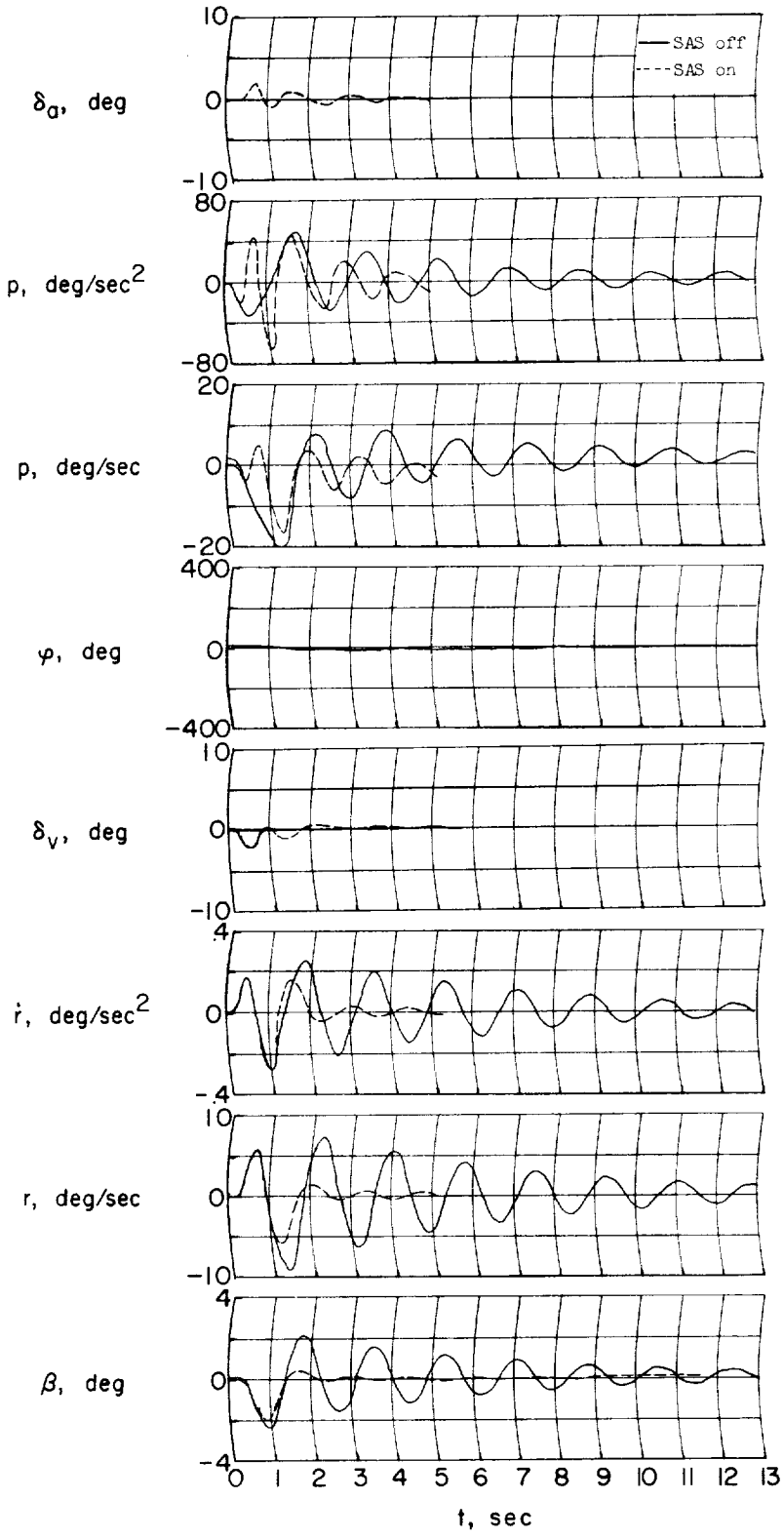

Figure 25.- Time histories of analog lateral pulses.

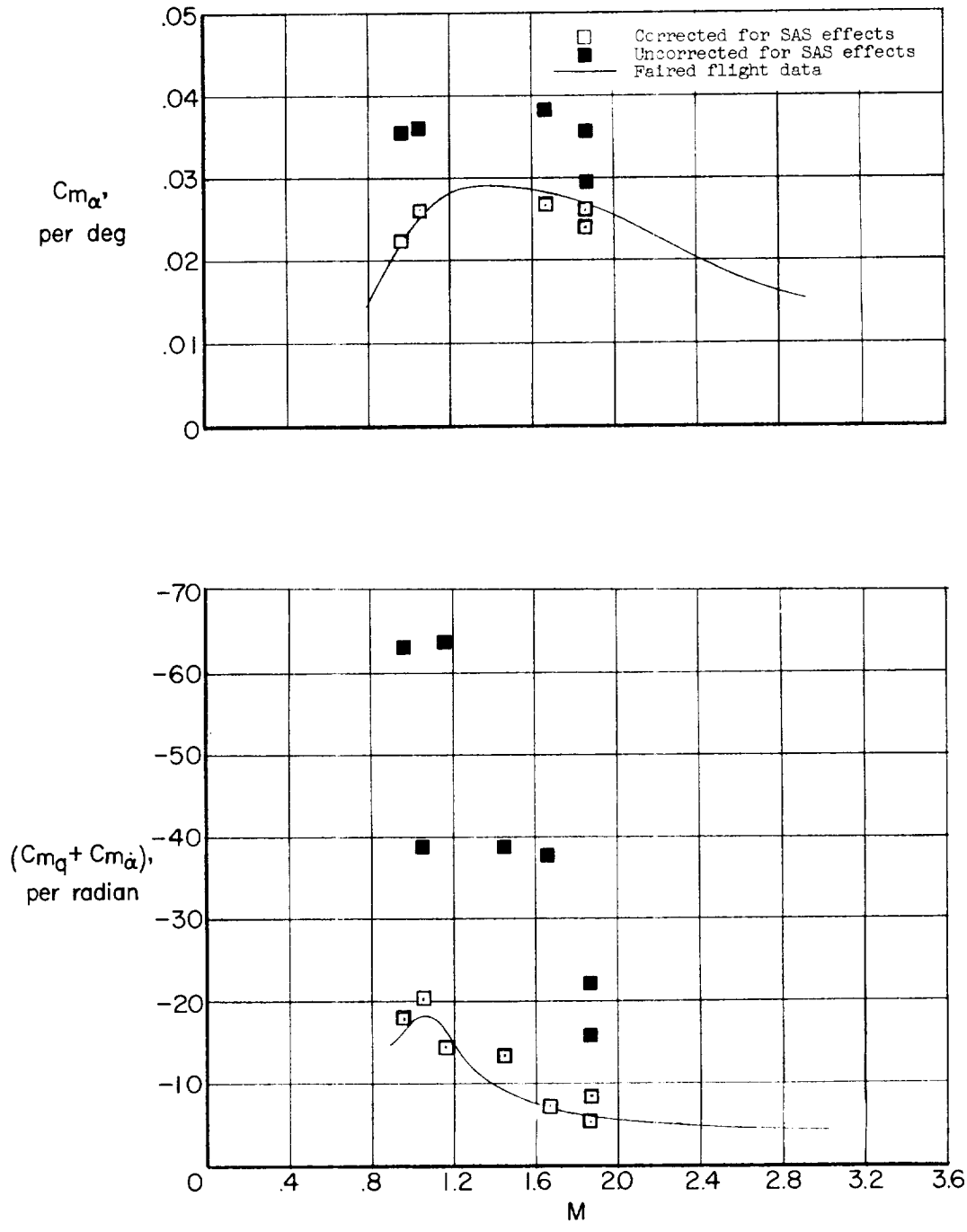

Figure 26.- Effects of stability-augmentation-system correction on C_{m_α} and $\left(C_{m_q} + C_{m_{\dot\alpha}}\right)$.

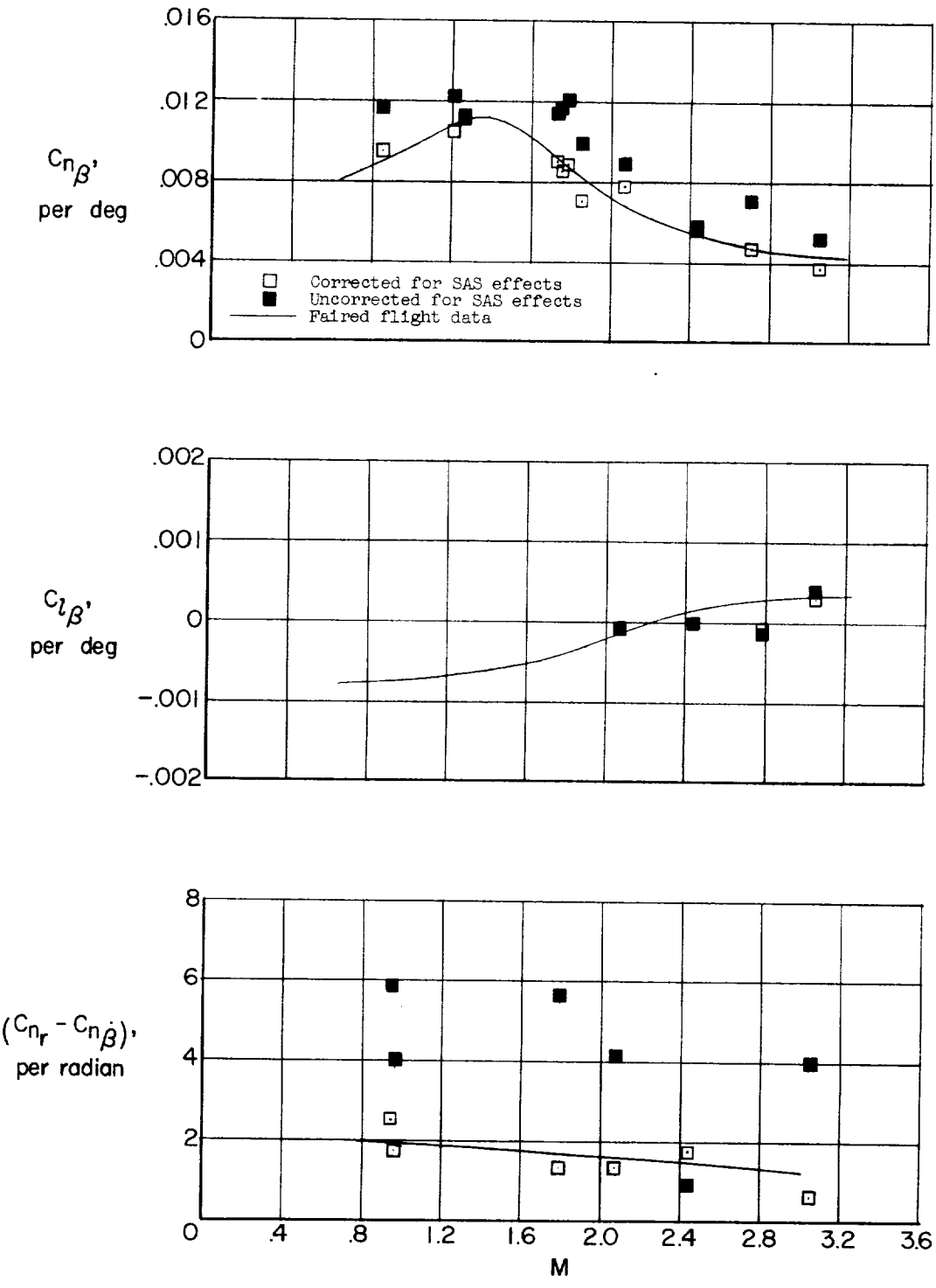

Figure 27.- Effects of stability-augmentation-system correction on C_{n_β}, C_{l_β}, and $\left(C_{n_r} - C_{n_{\dot\beta}}\right)$.